

Design, Synthesis and Pharmacological Evaluation of Novel N-Acylhydrazone Derivatives as Potent Histone Deacetylase 6/8 Dual Inhibitors.

Daniel Alencar Rodrigues, Guilherme Ferreira-Silva, Ana Carolina Ferreira, Renan Fernandes, J. K. Kwee, Carlos Maurício R Sant'Anna, Marisa Ionta, and Carlos Alberto Manssour Fraga

J. Med. Chem., **Just Accepted Manuscript** • Publication Date (Web): 24 Dec 2015

Downloaded from <http://pubs.acs.org> on December 24, 2015

Just Accepted

"Just Accepted" manuscripts have been peer-reviewed and accepted for publication. They are posted online prior to technical editing, formatting for publication and author proofing. The American Chemical Society provides "Just Accepted" as a free service to the research community to expedite the dissemination of scientific material as soon as possible after acceptance. "Just Accepted" manuscripts appear in full in PDF format accompanied by an HTML abstract. "Just Accepted" manuscripts have been fully peer reviewed, but should not be considered the official version of record. They are accessible to all readers and citable by the Digital Object Identifier (DOI®). "Just Accepted" is an optional service offered to authors. Therefore, the "Just Accepted" Web site may not include all articles that will be published in the journal. After a manuscript is technically edited and formatted, it will be removed from the "Just Accepted" Web site and published as an ASAP article. Note that technical editing may introduce minor changes to the manuscript text and/or graphics which could affect content, and all legal disclaimers and ethical guidelines that apply to the journal pertain. ACS cannot be held responsible for errors or consequences arising from the use of information contained in these "Just Accepted" manuscripts.

1
2
3 Design, Synthesis and Pharmacological Evaluation of Novel *N*-Acylhydrazone Derivatives as
4
5 Potent Histone Deacetylase 6/8 Dual Inhibitors
6
7
8
9

10 *Daniel A. Rodrigues,^{a, b} Guilherme A. Ferreira-Silva,^e Ana C. S. Ferreira,^f Renan A. Fernandes,^f*
11
12 *Jolie K. Kwee,^f Carlos M. R. Sant'Anna,^{a, d} Marisa Ionta,^e Carlos A. M. Fraga^{*, a, b, c}*
13
14
15
16

17 ^aLaboratório de Avaliação e Síntese de Substâncias Bioativas (LASSBio), Instituto de Ciências
18 Biomédicas, Universidade Federal do Rio de Janeiro, PO Box 68023, 21941-902, Rio de Janeiro,
19
20 RJ, Brazil
21
22
23

24 ^bPrograma de Pós-Graduação em Química, Instituto de Química, Universidade Federal do Rio de
25 Janeiro, 21941-909, Rio de Janeiro, RJ, Brazil
26
27
28

29 ^cPrograma de Pós-Graduação em Farmacologia e Química Medicinal, Instituto de Ciências
30 Biomédicas, Universidade Federal do Rio de Janeiro, 21941-902, Rio de Janeiro, RJ, Brazil
31
32
33

34 ^dDepartamento de Química, Instituto de Ciências Exatas, Universidade Federal Rural do Rio de
35 Janeiro, 23970-000, Seropédica, RJ, Brazil
36
37
38

39 ^eLaboratório de Biologia Animal Integrativa, Departamento de Biologia Celular e do
40 Desenvolvimento, Instituto de Ciências Biomédicas, Universidade Federal de Alfenas, 37130-
41
42 000, Alfenas, MG, Brazil
43
44

45 ^fCoordenação de Pesquisa, Instituto Nacional de Câncer, 20231-050, Rio de Janeiro, RJ, Brazil
46
47
48
49
50
51
52

53 KEYWORDS: HDAC, *N*-acylhydrazone, Cancer, Hepatocellular carcinoma
54
55
56
57
58
59
60

ABSTRACT

This manuscript describes a novel class of *N*-acylhydrazone (NAH) derivatives that act as histone deacetylase (HDAC) 6/8 dual inhibitors and were designed from the structure of trichostatin A (**1**). *Para*-substituted phenyl-hydroxamic acids presented a more potent inhibition of HDAC6/8 than their *meta* analogs. In addition, the effect of compounds (*E*)-4-((2-(4-(dimethylamino)benzoyl)hydrazono)methyl)-*N*-hydroxybenzamide (**3c**) and (*E*)-4-((2-(4-(dimethylamino)benzoyl)-2-methylhydrazono)methyl)-*N*-hydroxybenzamide (**3f**) on the acetylation of α -tubulin revealed an increased level of acetylation. These two compounds also affected cell migration, indicating their inhibition of HDAC6. An analysis of the antiproliferative activity of these compounds, which presented the most potent activity, showed that compound **3c** induced cell cycle arrest and **3g** induced apoptosis through caspase 3/7 activation. These results suggest HDAC6/8 as a potential target of future molecular therapies for cancer.

INTRODUCTION

Two families of enzymes regulate histone acetylation patterns: histone acetyltransferases (HATs), which catalyze the transfer of an acetyl group to the lysine residues in the *N*-terminal tails, and histone deacetylases (HDACs), which remove the acetyl groups of these proteins.¹ The balance between the acetylation and deacetylation of histones affects the structure of chromatin because an imbalance between these processes disrupts the interaction of histones with DNA. HDAC removes an acetyl group, resulting in a compact chromatin state and thereby silencing gene expression.^{1,2} In addition, some HDACs regulate the function of non-histone proteins, e.g., cytoplasmic proteins and transcription factors.³

Eighteen HDACs have been identified in the human genome, and these enzymes can be further divided into two large groups: zinc-dependent HDACs and nicotinamide adenine dinucleotide (NAD⁺)-dependent HDACs, which are known as sirtuins (class III). In addition, the zinc-dependent HDACs can be further divided into classes and subclasses: class I (HDAC1, HDAC2, HDAC3 and HDAC8), class IIa (HDAC4, HDAC5, HDAC7 and HDAC9), class IIb (HDAC6 and HDAC10), and class IV (HDAC11).^{3,4}

HDACs have been identified as remarkable drug targets in a novel therapeutic approach for the treatment of cancer and related diseases because HDAC inhibition results in the growth arrest, differentiation and apoptosis of many transformed cells.⁵⁻⁸ At present, four HDAC inhibitors (HDACI) have been approved through the *Food and Drug Administration* (FDA) (Figure 1). Vorinostat (SAHA) was approved in 2006 for the treatment of cutaneous T cell lymphoma (CTCL).⁹ Subsequently, romidepsin (FK-228)^{10,11} and belinostat (PXD-101)¹² were approved for the treatment of peripheral T-cell lymphoma (PTCL), and in 2015, panobinostat (LBH-589) was approved for the treatment of multiple myeloma.¹³

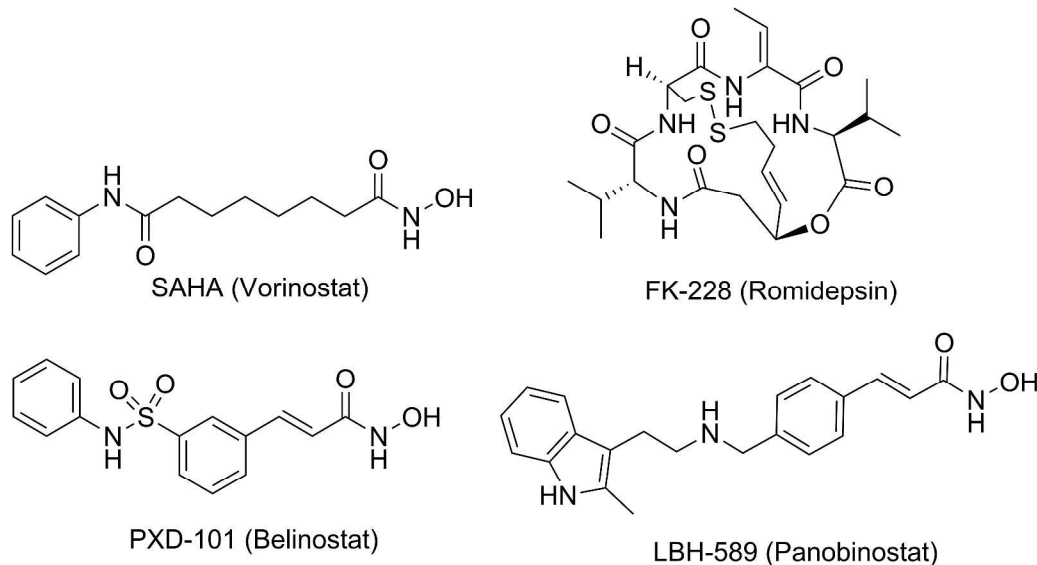


Figure 1. Chemical structures of FDA-approved HDAC inhibitors.

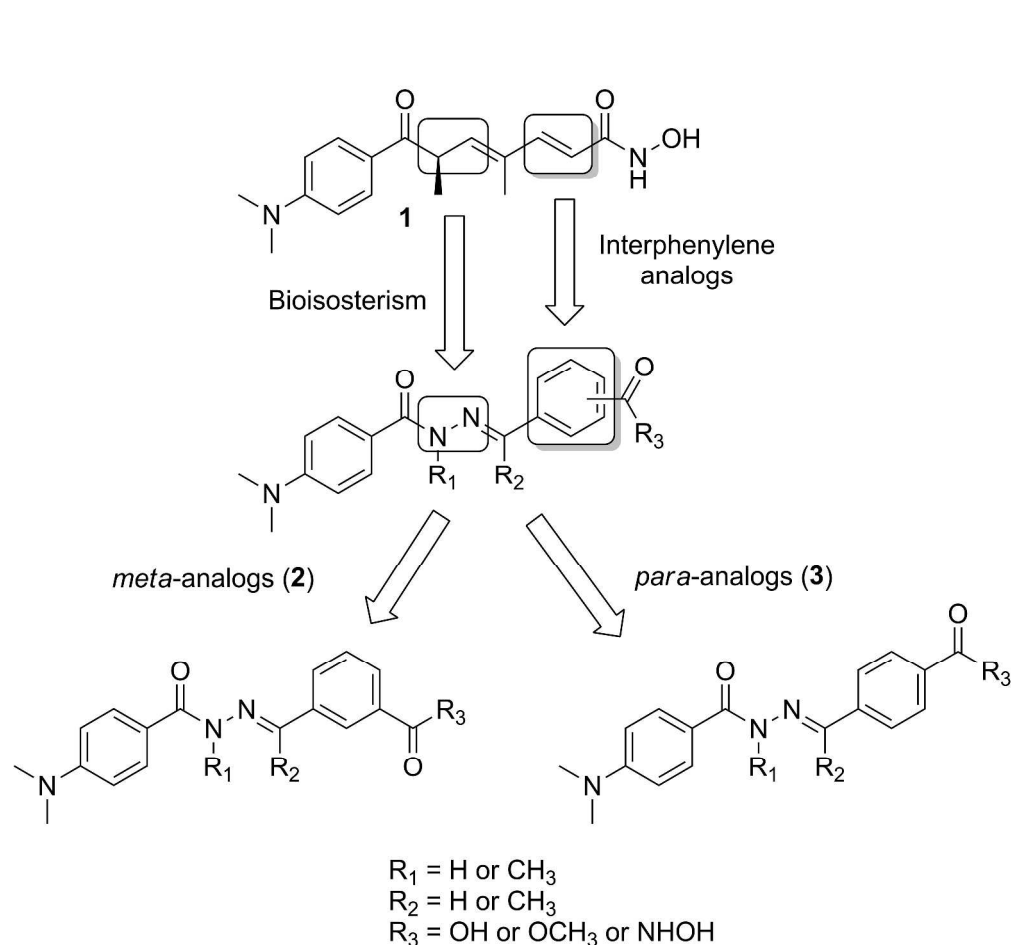
Although these compounds are structurally distinct, most HDACIs possess a well-known pharmacophore comprising a zinc-binding group (ZBG), a linker and a cap group to allow interactions at protein surface.^{5,7,14,15} Notably, no selective HDACIs have been approved for clinical use because all approved drugs have been characterized as pan-inhibitors of many different HDAC isoforms.

This manuscript describes the structural design, synthesis, *in vitro* pharmacological profile, and molecular modeling of a novel class of *N*-acylhydrazone (NAH) derivatives that act as HDAC 6/8 dual inhibitors. Selective inhibitors of HDAC6 or HDAC8 are already described.¹⁶⁻¹⁸ The selective inhibition of HDAC6 has proved a useful strategy for the treatment of a wide variety of solid and hematological tumors, wherein the antitumor effects observed through the selective inhibition of HDAC6 may be due to multiple mechanisms related to modulation of cytoplasmic proteins, that result in changes in the behavior of migration, motility and invasion of

1
2
3 cells.^{16,19} Furthermore, the selective inhibition of HDAC8, has been an attractive target for the
4
5 treatment of neuroblastoma, T-cell lymphoma and hepatocellular carcinoma (HCC).^{18,20,21} Both
6
7 HDAC6 and HDAC8 have been related with increased breast cancer cells invasion, increasing
8
9 the interest for compounds with such profile.²² It has been suggested that the dual inhibition of
10
11 HDAC6/8 approach has a great therapeutic potential, resulting in a large therapeutic window and
12
13 a profile of additive or synergistic effects which can benefit the treatment of various
14
15 malignancies e.g., neuroblastoma, T-cell lymphoma and HCC.^{23,24}
16
17
18
19
20
21

22 RESULTS AND DISCUSSION

23
24 **Design.** The compounds characterized in the present study were designed based on the structure
25
26 of trichostatin A (TSA) (**1**), a natural pan-HDAC inhibitor.²⁵ The classical bioisosteric
27
28 replacement of two *CH* moieties with *N* was used as the primary molecular modification strategy
29
30 for the synthesis of **1**'s derivatives.^{26,27} We exploited the *N*-acylhydrazone subunit (NAH), which
31
32 has been identified as a privileged structure,²⁸ for the design of new analogs (Figure 2).
33
34
35
36
37
38
39
40
41
42
43
44
45
46
47
48
49
50
51
52
53
54
55
56
57
58
59
60



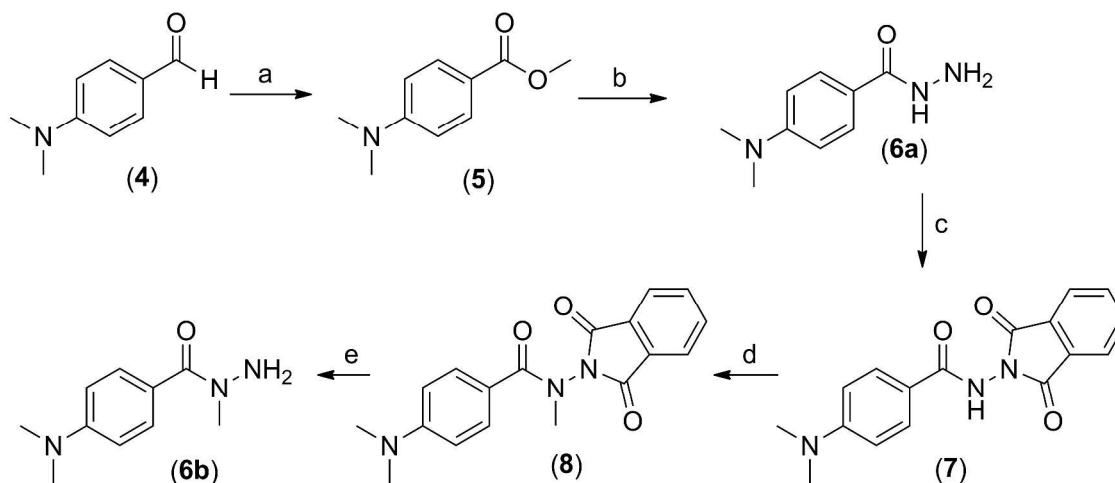
33 **Figure 2.** Design concept used to generate a novel class of NAH derivatives for the inhibition of
34 HDACs.
35

36
37
38
39
40 We replaced the unsaturation region conjugated to the hydroxamic acid with an
41 interphenylene linker. Although three regioisomers could be used for the new analogs (*ortho*-,
42 *meta*- and *para*-substituted), this design primarily focused on the use of *meta* (**2**) and *para* (**3**)
43 analogs because *ortho*-substituted compounds find it difficult to enter the channel in the HDAC
44 structure.
45
46
47
48
49

50
51 We also explored the influence of alkylation at R_1 and R_2 (R_1 and $R_2 = \text{H or Me}$) because
52 *N*-methylation of the NAH subunit could lead to conformational changes that may result in a
53 different pharmacological profile.^{29,30} Moreover, we evaluated carboxylic acids, esters and
54
55
56
57
58
59
60

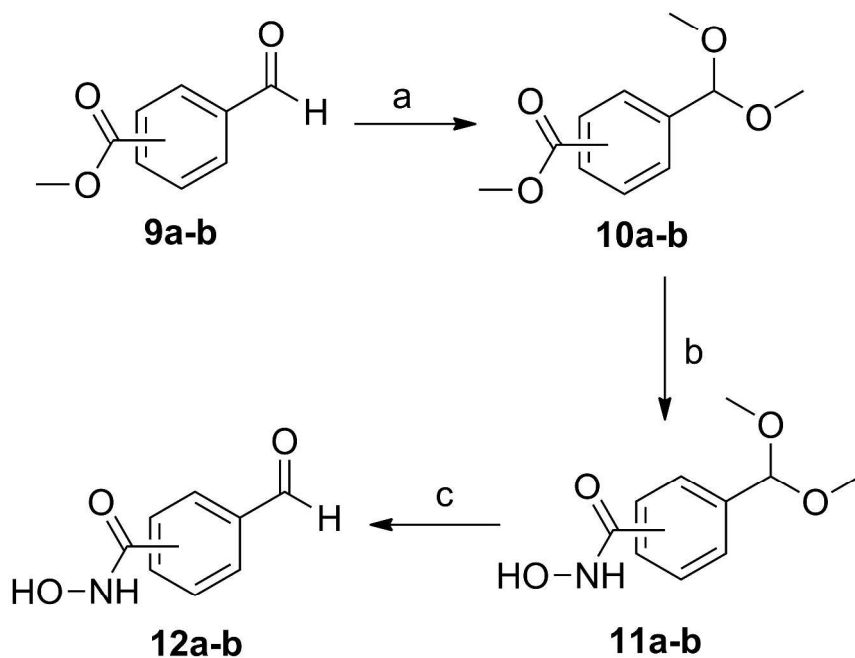
1
2
3 hydroxamic acids as zinc-binding groups to confirm the pharmacophoric behavior of these
4
5 chelating subunits.³¹
6
7
8
9

10 **Chemistry.** The target NAH series **2a-2f** and **3a-3f** were synthesized according to the procedures
11 depicted in Schemes 1–4. The desired NAH derivatives were constructed using a convergent
12 route, divided into the synthesis of the two main building blocks, i.e., the acylhydrazines **6a** and
13 **6b** and the respective aromatic aldehyde intermediates. Intermediate **6a** was obtained at 54%
14 yield (2 steps) through the oxidative processing of aldehyde **4** as described by Yamada and co-
15 workers,³² who added iodine to a potassium hydroxide methanolic solution and then performed a
16 hydrazinolysis reaction using hydrazine hydrate in methanol (Scheme 1). The synthesis of *N*-
17 methyl-acylhydrazine **6b** was achieved through the protection of the terminal amino group of
18 intermediate **6a** using phthalic anhydride followed by the base-catalyzed methylation of the
19 amide nitrogen with methyl iodide and the subsequent removal of the protecting group using
20 hydrazine hydrate in methanol (Scheme 1). After these three steps, acylhydrazine **6b** was
21 obtained at 55% yield.
22
23
24
25
26
27
28
29
30
31
32
33
34
35
36
37
38
39
40
41
42
43
44
45
46
47
48
49
50
51
52
53
54
55
56
57
58
59
60

Scheme 1^a

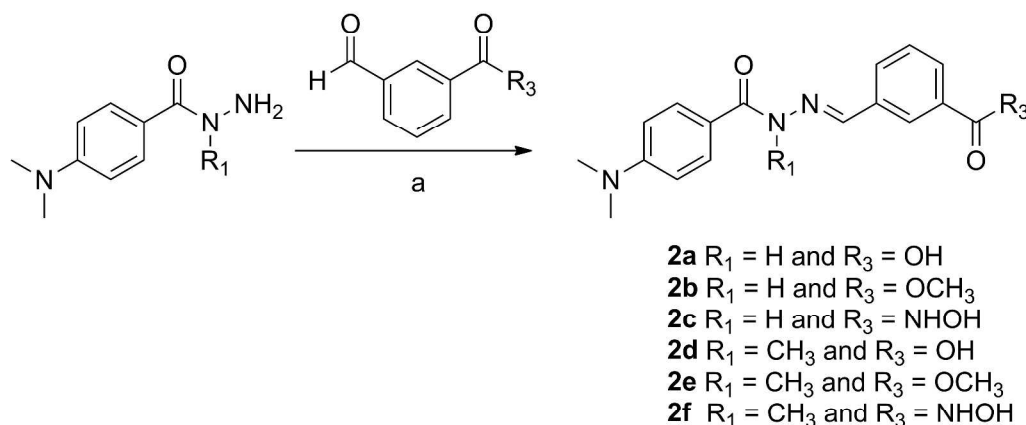
^aReagents and conditions: (a) I₂, KOH, MeOH, 0 °C, 10 h, 57%; (b) NH₂NH₂·H₂O, MeOH, 70 °C, 18 h, 95%; (c) phthalic anhydride, 180 °C, 2 h, 76%; (d) CH₃I, K₂CO₃, acetone, 50 °C, 18 h, 92%; (e) NH₂NH₂·H₂O, MeOH, 70 °C, 2 h, 79%

The aromatic aldehydes **12a** and **12b** were prepared from the corresponding benzaldehydes functionalized with ester groups. First, the aldehyde carbonyl group was protected using 2,2-dimethoxypropane under acid catalysis. A hydroxamic acid moiety was then introduced after the treatment of the acetal-esters **10a** and **10b** with hydroxylamine under basic conditions. Subsequently, the acetal group on hydroxamic acids **11a** and **11b** was hydrolyzed using sulfuric acid diluted in acetone, generating the corresponding functionalized benzaldehydes at yields ranging from 67 to 69% (three steps).

Scheme 2^a

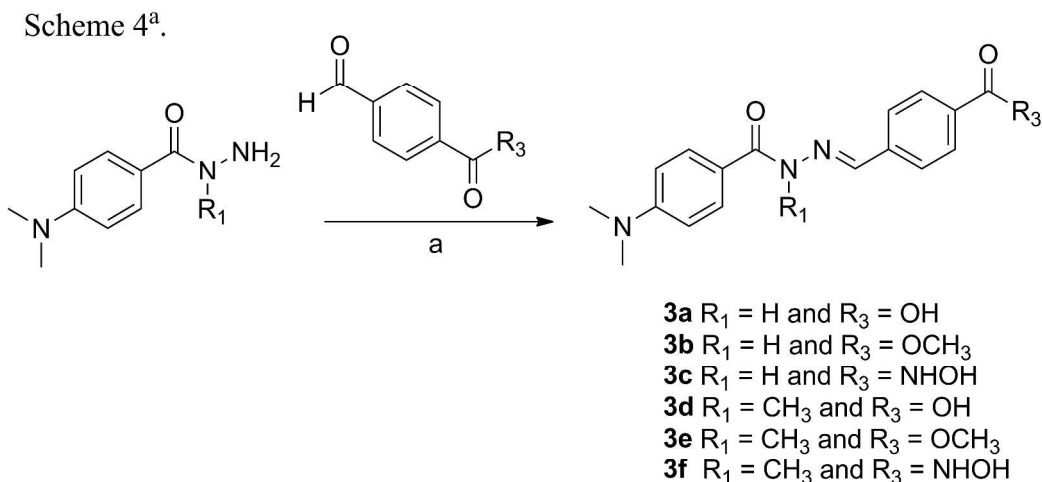
^aReagents and conditions: (a) 2,2-dimethoxypropane, TsOH_{cat.}, MeOH, r.t., 2 h, 82-85%; (b) NH₂OH·HCl, KOH, MeOH, r.t., 4 h, 90-94%; (c) H₂SO₄ 15% (w/v), acetone, r.t., 2 h, 87-91%.

Thus, the NAH derivatives **2a–2f** and **3a–3f** were prepared at high yields through the acid-catalyzed condensation of acylhydrazines **6a** and **6b** using the appropriate aromatic aldehydes, as illustrated in Schemes 3 and 4.

Scheme 3^a.

^aReagents and conditions: (a) HCl_{cat.}, EtOH, r.t., 2 h, 82-98%;

A careful analysis of the ¹H NMR spectra of the NAH derivatives **2a–2f** and **3a–3f** revealed the formation of a single diastereomer based on the presence of a single imine hydrogen signal, reflecting the relative configuration of the isomer (*E*). Previous studies have described this configuration for different bioactive *N*-acylhydrazone and *N*-methyl-*N*-acylhydrazone derivatives, as determined through ¹H NMR and X-ray analyses.^{30,33,34} In addition, we performed a NOEdiff (NOE-difference spectroscopy) experiment using the NAH derivative **3c** and the *N*-methyl-NAH **3f**. The spectra were collected after irradiation at the imine hydrogen and the substituent in the R₁ position (**3c** = H and **3f** = CH₃). We observed a relationship indicating a structural proximity between these atoms, further confirming the relative configuration (*E*) at the imine double bond of the NAH moiety (see Figures S15-S18, Supporting information).



^aReagents and conditions: (a) HCl_{cat.}, EtOH, r.t., 2 h, 62-89%;

HDAC inhibition. All of the *N*-acylhydrazone derivatives from the first family, i.e., with a hydrogen atom as R₂ (see Figure 2), were assessed for their HDAC inhibitory activity. First, the inhibitory activity of NAH was screened through a non-selective assay using rat liver HDACs.³⁵ Prior to this assay, we evaluated the solubility of these compounds in water (buffer pH 7.4) to ensure that the inhibition percentage values were not incorrectly interpreted due to precipitation of the compound in the reaction medium. Table 1 shows the inhibition percentage of rat liver HDACs induced by the *N*-acylhydrazones **2a-2f** and **3a-3f** at a concentration of 1 μM and the solubility of these compounds in water.

Table 1. HDAC inhibition, as assessed in rat liver HDACs, and aqueous solubility of each NAH compound.

Compound	% inhibition of HDAC (1 μM) ^a	HDAC rat liver inhibition, IC ₅₀ (μM) ^b	Aqueous solubility (μM) ^c
2a	-11.0	N.D.	> 70

2b	-4.6	N.D.	3.7
2c	66.0	1.2±0.047	> 67
2d	-5.8	N.D.	> 67
2e	-10.8	N.D.	8.2
2f	33.4	N.D.	> 70
3a	-9.1	N.D.	> 77
3b	-10.6	N.D.	1.7
3c	90.4	0.021±0.003	15
3d	-8.7	N.D.	> 67
3e	-11.6	N.D.	1.4
3f	90.4	0.018±0.0001	> 64

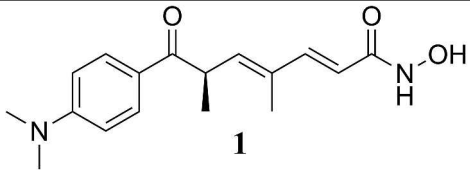
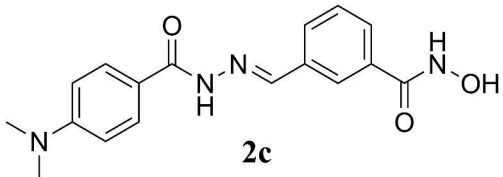
^aThe values presented are the average of two experiments. The data are shown as % inhibition of HDAC. ^bThe IC₅₀ values displayed are the mean of two experiments ± standard deviation in μM. The compounds were examined through a six-point enzyme assay with a three-fold serial dilution starting from 3 μM for **2c** and 1 μM for **3c** and **3f**. ^cDetermined using the spectrophotometric method developed by Schneider and coworkers.^{36,37} N.D. = not determined.

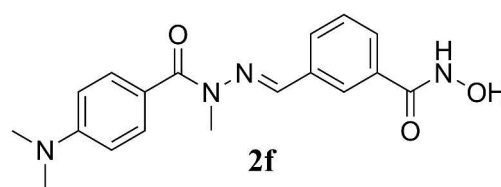
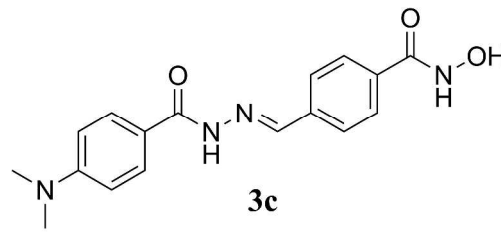
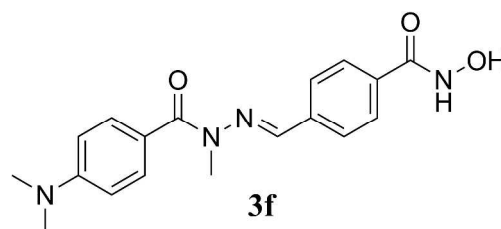
Compounds **2c**, **2f**, **3c** and **3f** presented 66.0, 33.4, 90.4 and 90.4% HDAC inhibition, respectively. The compounds functionalized with carboxylic acid and esters groups were not active at the concentrations used in the assay, consistent with previous studies that demonstrated that carboxylic acid derivatives are only active at high micromolar concentrations.^{14,38} The rat liver HDAC inhibition achieved by compounds **2c**, **3c** and **3f** was determined (Table 1),

revealing the potency for **3c** and **3f**, with IC_{50} values in the low nanomolar range of 21 and 18 nM, respectively.

The selectivity profile of the most active NAH derivatives, namely **2c**, **2f**, **3c** and **3f**, was evaluated in the main human HDAC isoforms, namely class I and class IIb.³⁹ Table 2 shows the IC_{50} values obtained for these NAH derivatives against HDAC1, 2, 6 and 8.

Table 2. Inhibitory profile of NAH derivatives **2c**, **2f**, **3c**, **3f** and trichostatin A (**1**) against human HDAC 1, 2, 6 and 8.

Inhibition of human HDAC isoforms, IC_{50} (μM) ^a				
Compound	HDAC 1	HDAC 2	HDAC6	HDAC8
	0.0085±0.001	0.052±0.008	0.009±0.002	0.36±0.015
	>10.0	>10.0	0.39±0.04	2.2±0.23

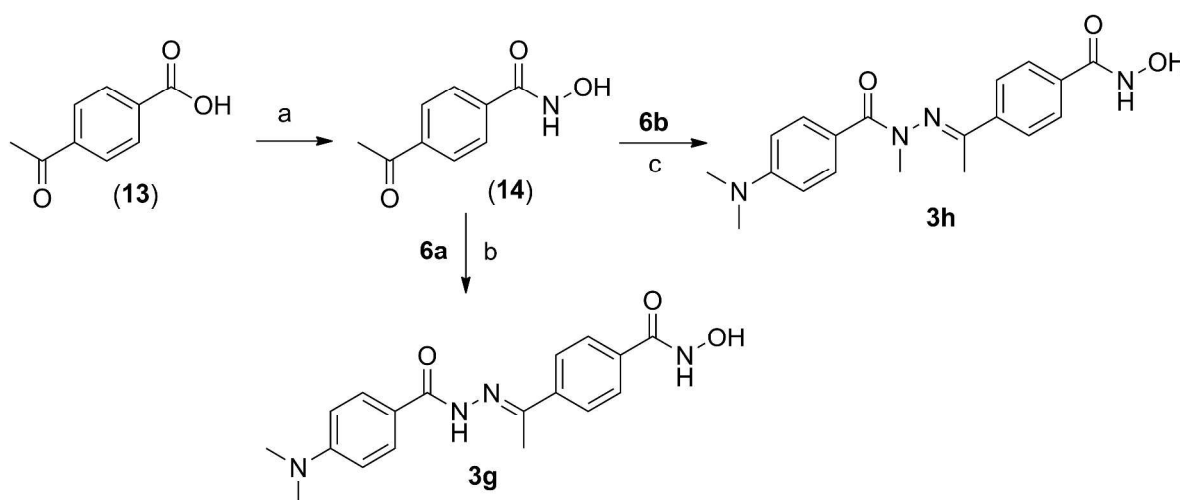
	>10.0	>10.0	2.5±0.21	2.0±0.36
	>3.0	>3.0	0.015±0.003	0.23±0.012
	>3.0	>3.0	0.027±0.011	0.13±0.026

^aThe IC₅₀ values displayed are the mean of three experiments ± standard deviation in μM. The compounds were examined through a seven-point enzyme assay with a three-fold serial dilution starting from 10 μM for **2c** and **2f** and 3 μM for **3c** and **3f**.

Both compounds presented here were selective for HDAC6 and HDAC8, although **3c** and **3f** were extremely potent, with IC₅₀ values in the low nanomolar range. For this family of compounds, we hypothesized that the reduced potency of the substituents in the *meta* position was associated with hydroxamic acid, whereas the substituents in the *para* position generated more potent compounds. The *N*-methylation of the *meta* analog (**2c** and **2f**) series decreases their ability to inhibit HDAC6. A similar finding was observed for the *para* analogs, although these compounds can be considered nearly equipotent.

To evaluate the influence of the methyl group in the R₂ position, we synthesized *para* analogs harboring this methyl group. The synthesis of **3g** and **3h** is shown in Scheme 5. Using 4-

1
2
3 acetyl-benzoic acid as the starting compound, we attempted to utilize the methodology applied
4
5 for the synthesis of the aldehyde intermediates; however, given the lower reactivity of ketones,
6
7 this strategy was not feasible. Therefore, we introduced the hydroxamic acid directly. The acid
8
9 **13** was subjected to acid chloride formation using oxalyl chloride. The intermediate was reacted
10
11 with hydroxylamine under basic conditions to generate acid **14** at 54% yield. The condensation
12
13 of the hydrazides (**6a** and **6b**) was performed in ethanol under microwave irradiation using
14
15 AcOH as the catalyst, which led to the generation of **3g** and **3h** at yields of 45 and 38%,
16
17
18
19
20
21
22
23
24
25
26
27
28
29
30
31
32
33
34
35
36
37
38
39
40
41
42
43
44
45
46
47
48
49
50
51
52
53
54
55
56
57
58
59
60

Scheme 5^a.

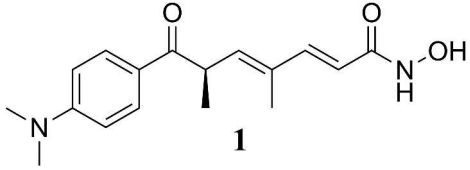
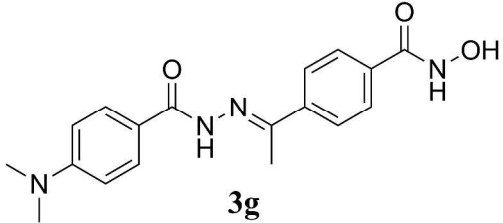
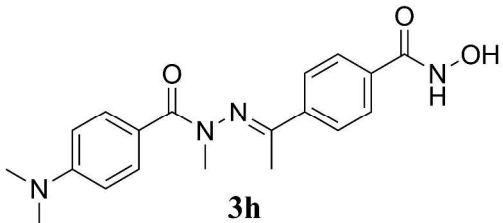
^aReagents and conditions: (a) Oxalyl chloride, DMF_{cat.}, DCM, r.t., 2 h, then 50 wt % NH₂OH, TEA, THF, 0 °C, 30 min, 54%. (b) AcOH_{cat.}, EtOH, 80 °C, MW, 30 min, 45%; (c) AcOH_{cat.}, EtOH, 125 °C, MW, 4 h, 38%;.

Analysis of the ¹H NMR spectra of **3g** and **3h** revealed the formation of a single isomer based on the presence of a single imino hydrogen signal, reflecting the (*E*)-isomer. A NOEdiff experiment (NOE-difference spectroscopy) was performed for **3g**. The spectra were collected

after irradiation at the hydrogen of the methyl group at the imino position and the R₁ position (**3g** = H), allowing us to observe the structural proximity between these atoms (see Figures S19 and S20, Supplementary information).

Prior to the pharmacological assay, we evaluated the solubility of **3g** and **3h** and found water solubility of 6.2 and 122 μM, respectively. The selectivity profile of **3g** and **3h** among HDACs of classes I and IIb was then determined, and Table 3 shows the IC₅₀ values of these compounds for HDAC1, 2, 6 and 8.

Table 3. Inhibitory profile of NAH derivatives **3g** and **3h** and trichostatin A (**1**) against human HDAC 1, 2, 6 and 8.

Inhibition of human HDAC isoforms, IC ₅₀ (μM)				
Compound	HDAC 1	HDAC 2	HDAC6	HDAC8
 1	0.0085±0.001	0.052±0.008	0.009±0.002	0.36±0.015
 3g	>3.0	>3.0	0.056±0.01	0.11±0.008
 3h	>3.0	>3.0	0.097±0.018	0.054±0.015

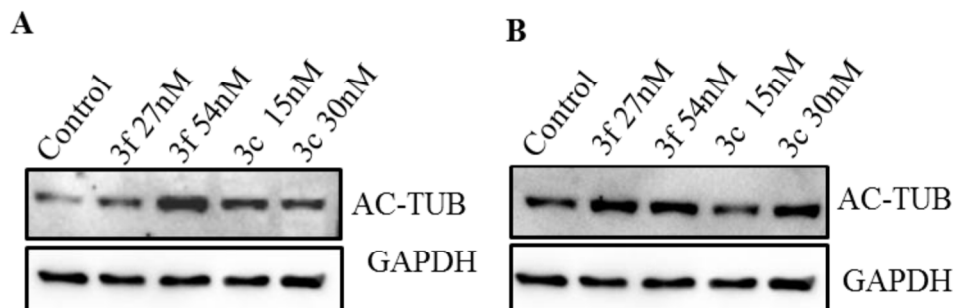
^aThe IC₅₀ values displayed are the mean of three experiments ± standard deviation in μM. The

1
2
3 compounds were examined through a seven-point enzyme assay with a three-fold serial dilution
4
5 starting from 3 μ M.
6
7

8
9
10 A methyl group in the R₂ position decreased the potency for HDAC6 inhibition, whereas
11 the presence of this moiety increased the HDAC8 inhibitory ability. The compound with a
12 methyl group in the R₁ and R₂ positions (**3h**) showed greater potency for HDAC8 inhibition
13 compared with the other analogs.
14
15
16
17
18

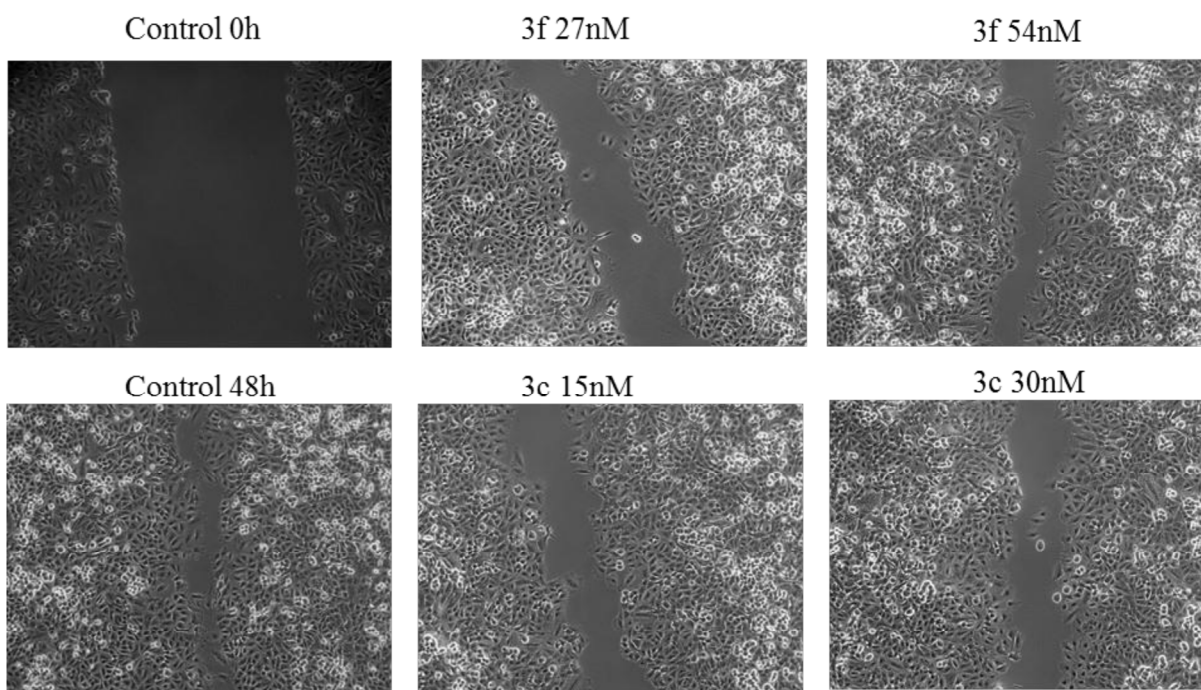
19
20 The selectivity of these compounds is influenced by the catalytic site of the HDACs.
21 Although the catalytic site is highly conserved, the rims of the catalytic channel of the HDAC
22 classes I and II have different dimensions. Because the channel of HDAC6 is wider and
23 shallower than that of HDAC1,⁴⁰ it is likely that aromatic linkers confer selectivity between these
24 isoenzymes, as previously described for phenyl-linked compounds, which have been
25 demonstrated to selectively inhibit HDAC6.^{23,41} The HDAC8 isoenzyme exhibits high
26 conformational flexibility, thereby accommodating a large variety of ligands, including phenyl-
27 linked compounds.⁴²
28
29
30
31
32
33
34
35
36
37

38
39 To confirm the inhibitory effects of **3c** and **3f** on HDAC6, the A549 and Calu-1 cell lines
40 were treated with these compounds, and the levels of acetylation in tubulin, a target of HDAC6,⁴³
41 were assessed through western blotting (Figure 3). Both compounds induced tubulin acetylation
42 in both tumor cell lines. Moreover, the effects of **3c** and **3f** on HDAC6 inhibition were found to
43 be correlated with cell migration. HDAC6 is considered the master regulator of cell migration,¹⁹
44 and the inhibition of this enzyme abrogates cancer cell migration (Figure 4).
45
46
47
48
49
50
51
52
53
54
55
56
57
58
59
60



15
16
17
18
19
20
21
22
23
24
25
26

Figure 3. HDACI enhances tubulin acetylation. Calu-1 (A) and A549 (B) cells were treated with compounds **3c** and **3f** for 24 h, and the levels of acetylated tubulin were assessed by western blotting. GAPDH was used as a loading control. One representative of three independent experiments is shown. Cells treated with vehicle (DMSO) were used as controls.



51
52
53
54
55
56
57
58
59
60

Figure 4. HDAC6 inhibition abrogates cell migration. Calu-1 cells were treated with compounds **3c** and **3f** for 48 h, and their migration was determined using the scratch test. One representative

1
2
3 of three independent experiments is shown. Cells treated with vehicle (DMSO) were used as
4
5 controls.
6
7

8
9
10 **Molecular modeling.** To understand how compounds **3c** and **3f** bind to these two HDAC
11 isoforms, we performed molecular docking simulations of these compounds into HDAC6 and
12 HDAC8 structures. Compounds **3c** and **3f**, which differ by the presence of a methyl group at R₁,
13 showed the best inhibition profiles, indicating that these two compounds represent the most
14 promising ligands investigated in the present study.
15
16
17
18
19
20
21

22 First, we focused on HDAC8 because many crystallographic structures of this isoform
23 have been deposited in the Protein Data Bank (PDB). Due to the high flexibility of the HDAC8
24 active site, it was necessary to carefully select the most adequate structure for this docking
25 study.⁴² We searched for co-crystals containing ligands with some structural similarity to the
26 tested compounds, particularly the phenyl-linked compounds. Two crystallographic structures
27 were selected: 1VKG (resolution: 2.20 Å)⁴² and 1W22 (resolution: 2.5 Å),⁴⁴ which contain the
28 ligands *N*^{4'}-hydroxy-*N*³,*N*³-dimethyl-5-(4-methylbenzamido)-[1,1'-biphenyl]-3,4'-dicarboxamide
29 (CRA-19156) and *N*-hydroxy-4-(*N*-methyl-5-(pyridin-2-yl)thiophene-2-sulfonamido)benzamide
30 (NHB), respectively.
31
32
33
34
35
36
37
38
39
40
41
42

43 Similar positions were observed for the compounds after docking into both HDAC8
44 structures, although here we only show the docking models for the CRA-19156 binding pocket
45 of HDAC8 (1VKG in PDB). As shown by the different conformational profiles of both ligands
46 presented in Figure 5 (see below), compounds **3c** and **3f** adopted different orientations in the
47 active site. Both compounds chelate with the zinc ion in the active site and form H-bonds with
48 His142, His143 and Tyr306 (Figures 5A and 5B), which are important residues in the catalytic
49
50
51
52
53
54
55
56
57
58
59
60

mechanism.⁴² Furthermore, these compounds undergo hydrophobic interactions through the phenyl linker with residues in the pockets of the wall (Phe152 and Phe208). Compound **3c** undergoes hydrogen bonding between the NH moiety of its NAH group and the carboxylate of residue Asp101, leaving the 4-dimethylamino-phenyl group in an essentially solvent-exposed orientation (Figure 5A), whereas **3f** assumes a bent conformation, creating more contacts with residues on the surface of HDAC8 (Figure 5B). Thus, the higher potency of **3f** is likely driven by entropy because interactions with the surface of the enzyme would dislocate more water molecules to the bulk of the solvent.

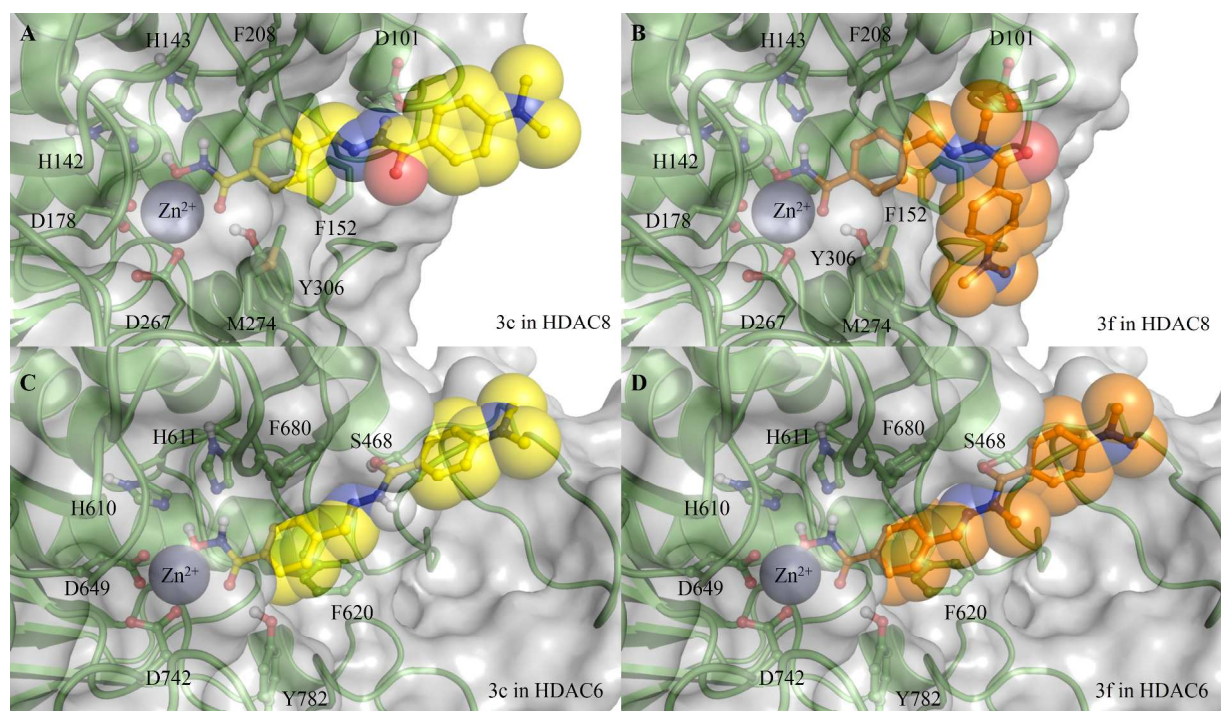


Figure 5. Predicted binding models of **3c** and **3f** in complex with HDAC8 (A, B) and HDAC6 (C, D), respectively. (A) and (B) Docking models of **3c** and **3f** in CRA-19156 binding pocket of HDAC8 (1VKG in PDB), respectively. (C) and (D) Docking models of **3c** and **3f** in the HDAC6

1
2
3 homology model built from HDAC7 (1C0Z in PDB), respectively. Docking studies were
4
5 performed by using the program GOLD 5.1.
6
7
8
9

10 Because there is no crystal structure for HDAC6, we constructed a homology model
11 using the SWISS-MODEL Workspace⁴⁵⁻⁴⁷ with an HDAC7 isozyme structure (1C0Z, resolution
12 = 2.10 Å) as the template.⁴⁸ For HDAC6, in addition to the pharmacophoric interactions, both
13
14
15
16
17
18
19
20
21
22
23
24
25
26
27
28
29
30
31
32
33
34
35
36
37
38
39
40
41
42
43
44
45
46
47
48
49
50
51
52
53
54
55
56
57
58
59
60

compounds have similar orientations in the active site, as shown in Figures 5C and 5D, reflecting the equipotency between these compounds.

Antiproliferative activity. Considering the promising results previously obtained, we evaluated the activity of some *para* analogs (**3c**, **3f**, **3g**, and **3h**) and *meta* analogs (**2c** and **2f**) on different tumor cell lines derived from melanoma, breast cancer, lung cancer and hepatocellular carcinoma (HCC) tissues. The compounds were initially screened at 40 μM, and cell viability was assessed after 48 h of treatment. The results showed that all of the tested compounds significantly reduced the viability of MCF-7, HT-144, and HepG2 cells in culture; however, the HT-144 and HepG2 cell lines were the most responsive to compounds **3c**, **3f**, **3g**, and **3h** (Figure 6). A dose-response curve was obtained to determine the IC₅₀ values, i.e., concentration necessary to inhibit 50% of cell growth. HT-144 and HepG2 cells were treated with compounds **3c**, **3f**, **3g**, and **3h** at different concentrations for 48 h. Lower IC₅₀ values were observed for the HepG2 cultures treated with compounds **3c** and **3g** (Table 4), suggesting the selectivity of these compounds for certain hepatocellular carcinoma cells. These results are interesting because HCC is one of the most malignant tumors, causing more than 600,000 deaths per year worldwide.⁴⁹ In addition, HDAC members, such as HDAC2, HDAC6, and HDAC8, are upregulated in HCC tissues and

cell lines, indicating that their close association with the proliferative behavior and invasion/migration activity of hepatocellular carcinoma cells.^{21,50,51}

Although it is possible to observe discrepancy between the IC₅₀ values in assays using human HDAC6 and HDAC8 for the compounds of **3c** and **3f** (low nanomolar) and the potency in cellular assay (micromolar), similar behavior was observed by Bergman et al.⁵² The reduced potency cannot be attributed to permeability problems since the treatment of A549 and Calu-1 cells with nanomolar doses of **3c** and **3f** resulted in increased acetylation of α -tubulin. And therefore these differences must be related to the selective inhibition of HDAC6/8.

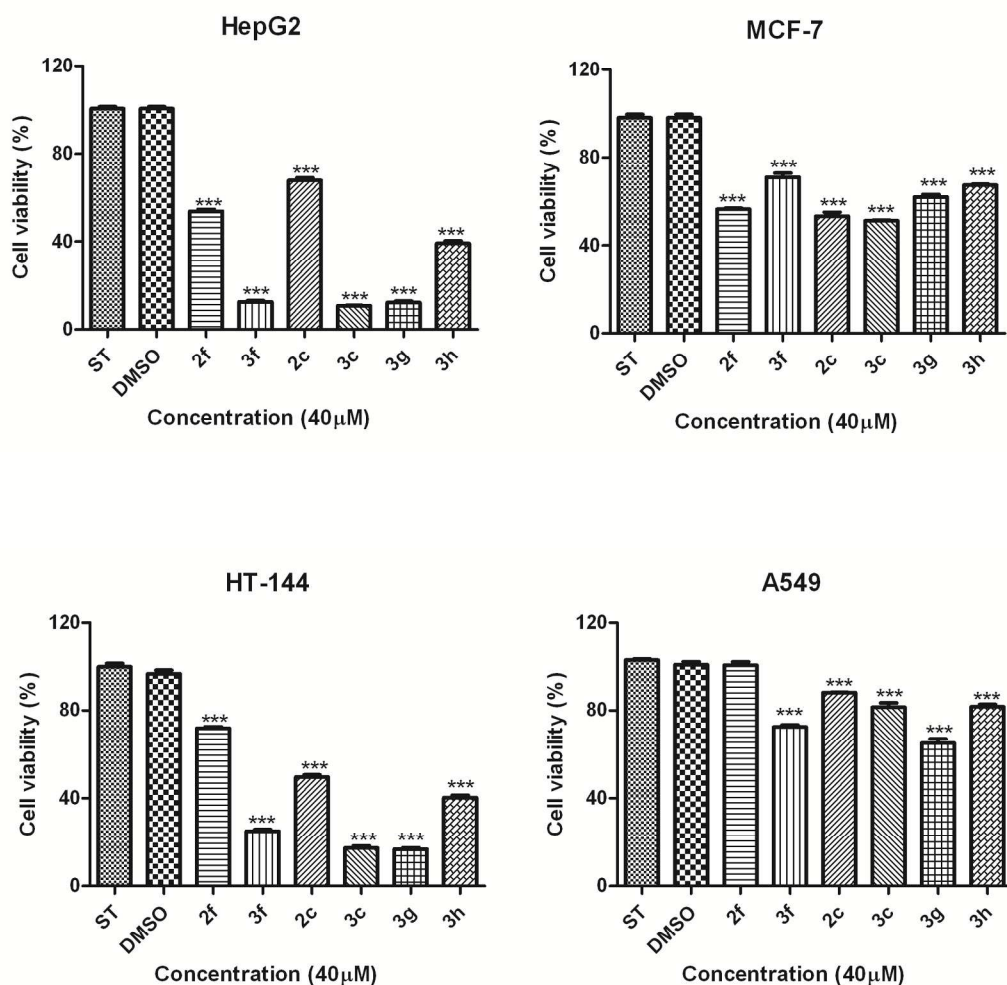


Figure 6. Cell viability determined using the MTS assay after 48 h of treatment with different compounds at 40 μM . The significance of the differences compared with the control groups were determined by ANOVA followed by Tukey's post-test. *** $p < 0.001$.

Table 4. IC_{50} values (μM) determined from data obtained through the MTS assay.

Compounds	Cell lines	
	HepG2	HT144
3c	9.48 ± 0.73	21.18 ± 0.69
3f	24.12 ± 0.87	36.10 ± 0.52
3g	11.52 ± 0.71	19.99 ± 0.64
3h	30.29 ± 1.38	51.64 ± 4.19

Due to the drastic reduction in cell viability after treatment with compounds **3c** and **3g** observed in HepG2 cell cultures, we investigated whether this event reflected the antiproliferative or cytotoxic potential of these compounds. To this end, we performed flow cytometry analyses to analyze the cell cycle progression of HepG2 cells treated with compounds **3c** and **3g** at concentrations of 5 and 10 μM for 24 and 48 h. Interestingly, the G2/M cell

1
2
3 population was significantly increased ($p < 0.001$) in cultures treated for 24 and 48 h with
4
5 compound **3c** at a concentration of 5 μM compared with the control group, whereas the
6
7 frequency of cells in the G0/G1 and S phases was decreased (Figure 7). We also observed a
8
9 gradual increase of the SubG1 population in cultures treated with compound **3c** compared with
10
11 the control cultures. This last event may reflect cell cycle arrest during either the G2/M transition
12
13 or the M phase. Further studies are needed to elucidate the precise point of the cell cycle at
14
15 which arrest is induced by compound **3c**. Studies have reported that the HDAC6 protein affects
16
17 the function of cytoplasmic non-histone proteins, including tubulin.^{53,54} In addition, disturbances
18
19 in the microtubule polarization dynamics lead to cell cycle arrest in the M phase, eventually
20
21 resulting in cell death. Zhang et al. (2003) reported that HDAC6 interacts with purified tubulin
22
23 and microtubules *in vitro* and that the inhibition of HDAC through TSA increases tubulin
24
25 acetylation.⁵⁵ Blagosklonny et al. (2002) showed that HDAC inhibitors differentially induce
26
27 tubulin acetylation, mitotic arrest, and cytotoxicity.⁵⁶ Because compound **3c** presented selective
28
29 inhibitory activity for HDAC6/8, it is likely that the increased G2/M population reflects
30
31 alterations in microtubule dynamics. However, additional experiments are needed to confirm this
32
33 hypothesis.
34
35
36
37
38
39
40
41
42
43
44
45
46
47
48
49
50
51
52
53
54
55
56
57
58
59
60

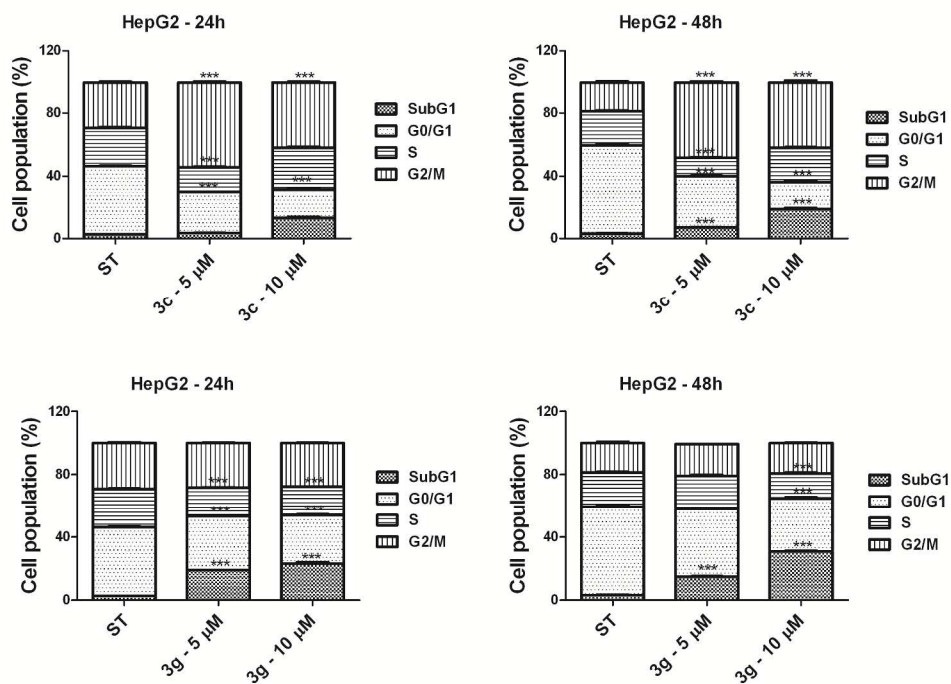
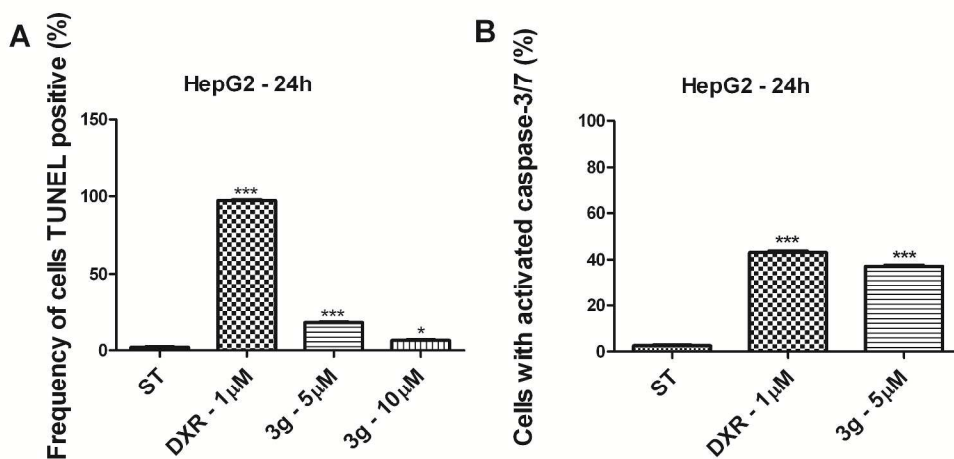


Figure 7. Cell cycle analysis of HepG2 cells treated with compounds **3c** and **3g** at concentrations of 5 and 10 μM for 24 and 48 h. The significance of the differences compared with the control results were determined by ANOVA followed by Tukey's post-test. *** $p < 0.001$.

The cell cycle analysis of cultures treated with **3g** revealed that this compound exhibits prominent cytotoxic activity on HepG2 cells, as demonstrated by an increase in the frequency of the SubG1 population accompanied by a gradual decrease in the G0/G1 and S populations (Figure 7). Thus, we investigated the potential of compound **3g** to induce apoptosis in HepG2 cells through flow cytometry. The frequency of TUNEL-positive cells was higher in cultures treated for 24 h with compound **3g** at concentrations of 5 and 10 μM compared with the frequency observed in the control group (Figure 8A). We also evaluated the activation profile of caspase 3/7 in cultures treated with compound **3g** at a concentration of 5 μM , which resulted in approximately 20% DNA fragmentation. The frequency of cells with activated caspase 3/7 was

1
2
3 significantly higher in the treated cultures than in the control cultures (Figure 8B). These results
4 demonstrate the effective pro-apoptotic activity of compound **3g** on HepG2 cells after 24 h of
5 treatment. At the molecular level, HDAC inhibitors have been associated with both cell cycle
6 regulation and apoptosis induction.^{57,58} Previous studies have shown that HDAC inhibitors
7 regulate the expression of multiple apoptosis mediators, which subsequently induce caspase 3/7
8 activation.^{53,59,60}



37
38 **Figure 8.** Frequency of apoptotic cells determined through a TUNEL assay (A), and the caspase
39 3/7 activation profile (B) in HepG2 cell cultures treated for 24 h with compound **3g**. Doxorubicin
40 (DXR) was used as a positive control. The significance of the differences compared with the
41 control results were determined by ANOVA followed by Tukey's post-test. * $p < 0.05$ and *** p
42 < 0.001 .

43
44
45
46
47
48 **Chemical stability study.** Based on the pharmacological data, compounds **3c**, **3f**, **3g** and **3h** are
49 promising for the study of HDAC6/8 inhibitors. However, the presence of a methyl group may
50 impart unique characteristics to these compounds, as will be discussed later. Furthermore, these
51
52
53
54
55
56
57
58
59
60

1
2
3
4
5
6
7
8
9
10
11
12
13
14
15
16
17
18
19
20
21
22
23
24
25
26
27
28
29
30
31
32
33
34
35
36
37
38
39
40
41
42
43
44
45
46
47
48
49
50
51
52
53
54
55
56
57
58
59
60

compounds present an imine subunit, which may represent vulnerability to hydrolysis, leading to instability and limiting the development of these compounds as candidate drugs. However, the compounds in question are functionalized acylhydrazones, which are admittedly more stable than imines.⁶¹ Thus, to advance the development of the HDAC inhibitor compounds examined in the present study, we examined the chemical stability of the most promising compounds from the series, namely **3c**, **3f**, **3g** and **3h**, to evaluate the effect of *N*-methylation on the stability of these compounds.

We conducted this study under two conditions, pH 2.0 and pH 7.4, to mimic the acidic stomach and the neutral plasma environments, respectively. To this end, compounds **3c**, **3f**, **3g** and **3h** were examined in the presence of acidic (pH 2) and neutral (pH 7.4) buffers under stirring for 240 min at a controlled temperature (37 °C). The results are shown in Figure 9.

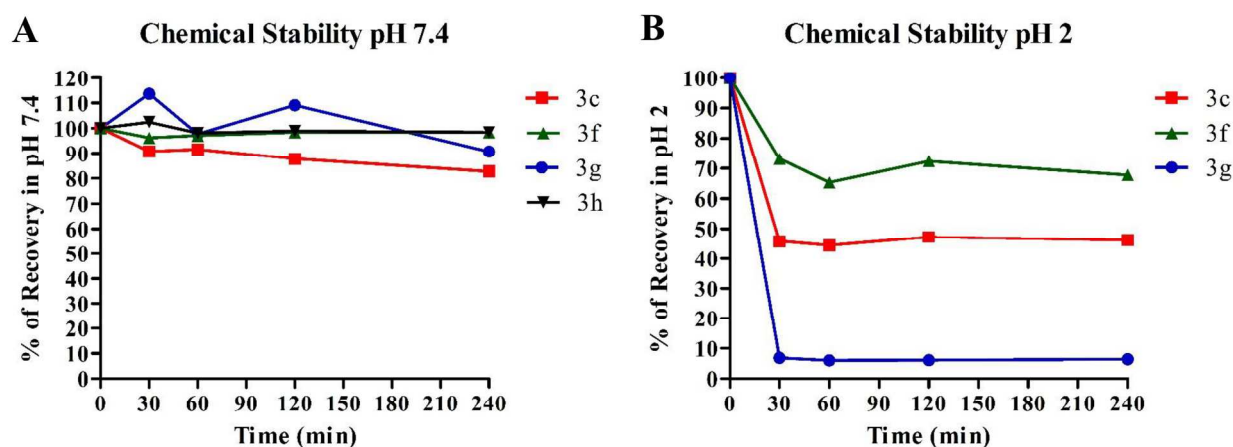
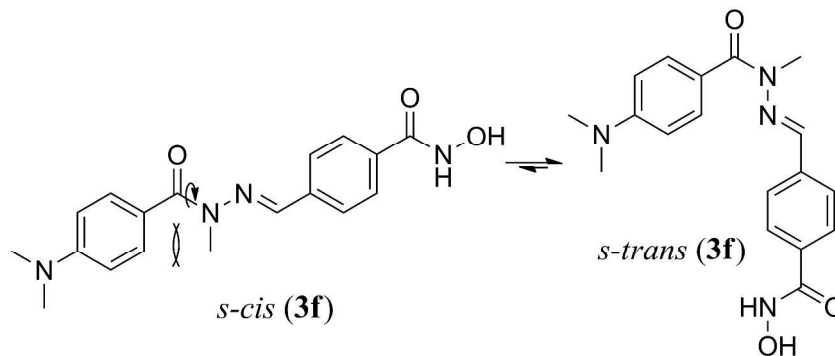


Figure 9. Chemical stability of compounds **3c**, **3f**, **3g** and **3h**. A) Chemical stability of compounds **3c**, **3f**, **3g** and **3h** at pH 7.4. B) Chemical stability of compounds **3c**, **3f**, **3g** and **3h** at pH 2. The experiments were conducted in triplicate, and the values shown represent the average from the experiments.

1
2
3 In the neutral medium (pH 7.4), all of the compounds were stable, with less than 15%
4 degradation (Figure 9A), as observed from the compound recovery percentage after 4 h.
5
6 However, in acidic buffer, all of the compounds underwent hydrolysis, although **3f** showed more
7 stability, with a higher percentage recovery of 70% after 4h, whereas the compounds with a
8 methyl group at the R₂ position (**3g** and **3h**) were highly unstable, and no significant quantities of
9 these compounds were recovered after 30 min. Notably, we recovered 6% of compound **3g** after
10 30 min, but after 4 h, we did not observe any amount of the compound (Figure 9B). The effect of
11 the methyl group on the stability of these compounds will be discussed later.
12
13
14
15
16
17
18
19
20
21
22
23

24 **The *N*-methylation conformational effect.** As previously described,²⁹ the *N*-methylation of *N*-
25 acylhydrazones changes the lowest energy conformation from *s*-cis to *s*-trans, as shown in
26 Scheme 6. Additionally, to reduce unfavorable steric contacts between the methyl and carbonyl
27 groups, the modeling results showed a loss of coplanarity between the carbonyl and the N-N=C
28 moieties, with a dihedral angle for O=C-N-N of 166.43° in the *N*-methylated structures. It is
29 expected that a reduction of coplanarity would decrease conjugation between the nitrogen lone
30 pair and the carbonyl portion of the *N*-acylhydrazone. The carbonyl carbon would become more
31 electron deficient, consistent with the chemical shift differences observed between the
32 compounds without the *N*-methyl group (**2a-2b**, **3a-3b** and **3g**; $\delta = 163$ ppm) and the *N*-
33 methylated compounds (**2d-2f**, **3d-3f** and **3h**; $\delta = 169$ ppm).
34
35
36
37
38
39
40
41
42
43
44
45
46
47
48
49
50
51
52
53
54
55
56
57
58
59
60

Scheme 6.



Moreover, weakened conjugation with the carbonyl group increases the availability of the electron pair on the nitrogen atom for conjugation with the imine portion of the *N*-acylhydrazone group. The observed effect of the increased electron density at the iminic carbon was a change in the chemical shift value for the series with $R_2 = \text{H}$ from $\delta = 145$ ppm (**2a-2c** and **3a-3c**) to $\delta = 138$ ppm (**2d-2f** and **3d-3f**). The presence of a methyl group at R_2 yielded the opposite effect: to avoid unfavorable steric interactions, a conformational change occurs, leading to a reduction in the conjugation of the *N*-acylhydrazone subunit and thereby reducing the electronic density in the imine carbon ($\delta = 152$ ppm; **3g**). Methylation at R_1 and R_2 further decreased conjugation, which was observed as a high chemical shift value for the imine carbon of $\delta = 167$ ppm (**3h**).

The electron density on the imine carbon may reflect the chemical stability of the *N*-acylhydrazones at acidic pH because a lower electron density at this carbon indicates that this atom is more electrophilic and available for nucleophilic attack by water. This behavior was demonstrated in the chemical stability studies of **3c**, **3f**, **3g** and **3h**, which revealed that compound **3f** was more chemically stable at pH 2.0.

Another important effect of the insertion of a methyl group is the increased water solubility of *N*-methylated compounds (**3f** and **3h**). Although the addition of a methyl leads to

1
2
3 increased lipophilicity, the methyl group insertion induces the “globular” conformation of the
4
5 compound, which is observed as a change in the lowest-energy conformation (*s-trans*). To
6
7 understand the high solubility of *N*-methyl derivatives (**3f** and **3h**), we determined the
8
9 experimental logD_{7,4} values for **3c** and **3f** and obtained values of 0.68 and 0.98, respectively. We
10
11 found that the addition of a methyl group expectedly increased lipophilicity but increased
12
13 solubility in water, an effect that cannot be correlated with lipophilicity. This behavior may
14
15 reflect an entropic effect because in aqueous solution, the compound is surrounded by a network
16
17 of water molecules, resulting in a smaller number of water molecules being necessary to solvate
18
19 the most globular compound. Furthermore, the higher water solubility of *N*-methyl-*N*-
20
21 acylhydrazone derivatives may reflect fewer or weaker intermolecular interactions established in
22
23 the crystal structure compared with compounds without the *N*-methyl group.
24
25
26
27
28

29 We also calculated the pK_a values for **3c** and **3f** using the method developed by Martinez
30
31 and Dardonville⁶² to reconcile the values obtained for logD_{7,4}. We determined that these
32
33 compounds are more acidic than expected with basis on a previously published work,⁶³ because
34
35 the values for both compounds were 8.1 and a large population of the molecules were detected in
36
37 ionized, water-soluble forms.
38
39
40
41
42

43 CONCLUSIONS

44
45
46 In this study a novel bioisoteric relationship between β,γ-unsaturated carbonyl framework
47
48 of natural product trichostatin A (**1**) and the privileged *N*-acylhydrazone moiety was
49
50 characterized, allowing us to obtain novel potent and selective HDAC 6/8 inhibitors. The
51
52 biological assays performed herein demonstrated that NAH derivatives **3c**, **3f**, **3g** and **3h**,
53
54 presenting the pharmacophoric hydroxamic acid moiety, exhibit important antitumor activities
55
56
57
58
59
60

1
2
3 against melanoma and hepatocellular carcinoma cells. Compound **3c** primarily induced cell cycle
4
5 arrest in the G2/M phase and eventual cell death in HepG2 cells, whereas compound **3g**
6
7 effectively induced apoptosis through caspase 3/7 activation. These results not only provide
8
9 further insight into the pathogenic mechanisms of HCC but also suggest HDAC6/8 as a potential
10
11 target of future molecular therapies for some kind of tumors.
12
13
14
15
16

17 EXPERIMENTAL SECTION

18
19
20 **General information.** The melting points of the intermediates were determined using a Quimis
21
22 340 apparatus and are uncorrected. The melting points of **2a-2f** and **3a-3f** were determined
23
24 through Differential Scanning Calorimetry (DSC) performed on a Shimadzu calorimeter (Model
25
26 DSC-60). The equipment was calibrated using an indium standard. The weight of the samples
27
28 was approximately 1.0 mg. The heating ramp was performed between 0 and 300 °C. The samples
29
30 were subjected to a heating rate of 20 °C per minute under nitrogen gas flow (50 mL/min) and
31
32 atmospheric pressure. The DSC pans with the samples were enclosed in a Shimadzu press
33
34 (model SSC-30). ¹H NMR spectra were determined in deuterated chloroform or dimethyl
35
36 sulfoxide containing approximately 1% tetramethylsilane (TMS) as an internal standard using a
37
38 Bruker DPX-200 at 200 MHz, DRX-300 at 300 MHz, Varian 400-MR at 400 MHz and Varian
39
40 500-MR at 500 MHz. ¹³C NMR spectra were determined using the same spectrometer at 50, 75,
41
42 100 and 125 MHz, respectively, and employing the same solvents. The NOEdiff experiment was
43
44 performed using a Varian Unity-300 at 300 MHz. IR spectra (cm⁻¹) were obtained using a
45
46 Thermo Scientific Nicolet module Smart ITR. The progress of all of the reactions was monitored
47
48 through thin-layer chromatography performed on 2.0 × 6.0-cm² aluminum sheets precoated with
49
50 silica gel 60 (HF-254, Merck) to a thickness of 0.25 mm. The developed chromatograms were
51
52
53
54
55
56
57
58
59
60

1
2
3 viewed under ultraviolet light (254–366 nm) and treated with iodine vapor. The reagents and
4
5 solvents were purchased from commercial suppliers and used as received. Analytical HPLC was
6
7 performed for compound purity determinations using a Shimadzu LC-20AD with a Kromasil
8
9 100-5C18 column (4.6 mm × 250 mm) and a Shimadzu SPD-M20A detector. The solvent system
10
11 used for the HPLC analyses was acetonitrile:water at 50:50 with or without of 0.5%
12
13 trifluoroacetic acid. The isocratic HPLC mode was used, and the flow rate was 1.0 mL/min. The
14
15 purity of the compounds was higher than 95%. Ultraviolet spectroscopy was performed using a
16
17 Femto spectrophotometer. The wavelength used in the solubility assay was determined as the
18
19 maximum λ characteristic of each compound. The spectra were analyzed using the Femto Scan
20
21 software. Mass spectrometry was performed through positive or negative ionization by Bruker
22
23 AmaZon SL, and the data were analyzed using the Compass 1.3.SR2 software.
24
25
26
27
28
29
30
31

32 **Methyl 4-(dimethylamino)benzoate (5).** Methanolic solutions (each 10 mL) of iodine (2.55 g,
33
34 10.05 mmol) and KOH (1.12 g, 20.1 mmol) at 0 °C were successively added to a solution of 4-
35
36 (dimethylamino)benzaldehyde (4) (0.5 g, 3.35 mmol) in absolute methanol (5 mL) cooled to 0
37
38 °C. After stirring for 10 h at 0 °C, 50 mL of saturated NaHSO₃ solution was added to the
39
40 reaction, resulting in the disappearance of the brown color. The methanol was then evaporated
41
42 under reduced pressure. The remaining content was stirred for 30 min at 0°C, and a white solid
43
44 precipitate was formed. The title compound was obtained through filtration and recrystallized in
45
46 ethanol/water as a white solid. Yield 0.34 g (57%); mp. 97 – 99 °C. ¹H NMR (400 MHz, CDCl₃):
47
48 δ 7.91 (d, 2H, J = 8.0 Hz), 6.66 (d, 2H, J = 8.0 Hz), 3.85 (s, 3H), 3.03 (s, 6H). ¹³C NMR (100
49
50 MHz, CDCl₃): δ 167.5, 153.2, 131.3, 117.2, 110.9, 51.5, 40.2. IR (ATR, cm⁻¹): 1697, 1278. MS
51
52 calculated for C₁₀H₁₃NO₂: [M]⁺ = 179.09. Found: [M + H]⁺ = 179.97.
53
54
55
56
57
58
59
60

1
2
3
4
5
6 **4-(Dimethylamino)benzohydrazide (6a)**. A total of 8.0 mL of hydrazine hydrate (163.5 mmol)
7
8 was added to a solution of **5** (2.9 g, 16.35 mmol) in absolute methanol (20 mL). The resulting
9
10 mixture was stirred at 70°C for 18 h. After cooling at room temperature, the methanol was
11
12 concentrated in a vacuum. The resulting white solid was filtrated and washed with 50 mL of
13
14 hexane and 50 mL of ethyl ether. The title compound was obtained after recrystallization in hot
15
16 ethanol as a white solid. Yield 2.77 g (95%); mp. 170 – 172 °C. ¹H NMR (400 MHz, DMSO-*d*₆):
17
18 δ 9.39 (br s, 1H), 7.69 (d, 2H, *J* = 8.0 Hz), 6.65 (d, 2H, *J* = 8.0 Hz), 4.33 (br s, 2H), 2.95 (s, 6H).
19
20 ¹³C NMR (50 MHz, DMSO-*d*₆) δ (ppm): 166.2, 152.0, 128.2, 119.5, 110.8, 39.6. IR (ATR, cm⁻¹):
21
22 3296, 3261, 3180, 1597. MS calculated for C₉H₁₃N₃O: [M]⁺ = 179.11. Found: [M + H]⁺ =
23
24 179.96.
25
26
27
28
29
30
31

32 **4-(Dimethylamino)-*N*-(1,3-dioxoisindolin-2-yl)benzamide (7)**. Phthalic anhydride (0.843g,
33
34 5.69 mmol) was added to a round-bottom flask, and this solid was stirred at 180°C until the solid
35
36 melted. Subsequently, **6a** (0.5 g, 2.85 mmol) was added to the flask without any added solvent,
37
38 and a yellow solid instantly formed. After the mixture was stirred at 180°C for 2 h, the solid was
39
40 triturated and subsequently stirred for 1 h at room temperature in 50 mL of saturated Na₂CO₃
41
42 solution. The solid was collected through filtration and washed with 50 mL of hexane and 50 mL
43
44 of ethyl ether. The title compound was obtained as a yellow solid. Yield 0.67 g (76%); mp. >250
45
46 °C. ¹H NMR (200 MHz, DMSO-*d*₆) δ 10.86 (br s, 1H), 8.06 - 7.88 (m, 4H), 7.82 (d, 2H, *J* = 8.0
47
48 Hz), 6.77 (d, 2H, *J* = 8.0 Hz), 3.01 (s, 6H). ¹³C NMR (50 MHz, DMSO-*d*₆) δ 165.8, 165.2, 153.1,
49
50 135.4, 129.6, 129.4, 123.8, 116.8, 110.8, 39.7. IR (ATR, cm⁻¹): 3275, 1732, 1654, 1599. MS
51
52 calculated for C₁₇H₁₅N₃O₃: [M]⁺ = 309.11. Found: [M + H]⁺ = 310.08.
53
54
55
56
57
58
59
60

1
2
3
4
5
6 **4-(Dimethylamino)-N-(1,3-dioxoisindolin-2-yl)-N-methylbenzamide (8)**. A solution of 7
8 (2.3 g, 7.44 mmol) and potassium carbonate (3.0 g, 22.32 mmol) were suspended in 20 mL of
9 acetone in a round-bottom flask. The suspension was thoroughly mixed under vigorous stirring
10 for 5 min, and methyl iodide (1.07 mL, 14.88 mmol) was subsequently added. The reaction was
11 heated at 50 °C and maintained under stirring for 18 h. Subsequently, the reaction was
12 evaporated under reduced pressure, and the residual solid was suspended in 2 mL of ethanol and
13 poured into cold water. The solid was collected through filtration, and the title compound was
14 obtained as a yellow solid. Yield 2.2 g (92%); mp. 165 – 168 °C. ¹H NMR (300 MHz, DMSO-
15 *d*₆) δ 8.01 - 7.83 (m, 4H), 7.32 – 7.14 (m, 2H), 6.63 – 6.41 (m, 2H); 3.25 (s, 3H), 2.85 (s, 6H).
16 ¹³C NMR (75 MHz, DMSO-*d*₆) δ 165.5, 151.8, 135.3, 129.2, 128.4, 123.8, 118.9, 110.6, 39.4.
17 The -NCH₃ signal likely has a chemical shift similar to the septet of DMSO-*d*₆, making this
18 effect difficult to view. IR (ATR, cm⁻¹): 1728, 1656, 1608. MS calculated for C₁₈H₁₇N₃O₃: [M]⁺
19 = 323.13. Found: [M + H]⁺ = 324.08.
20
21
22
23
24
25
26
27
28
29
30
31
32
33
34
35
36
37
38

39 **4-(Dimethylamino)-N-methylbenzohydrazide (6b)**. A total of 0.25 mL of hydrazine hydrate
40 100% (5.11 mmol) was added to a solution of **8** (1.55 g, 4.64 mmol) in absolute methanol (10
41 mL). The resulting mixture was stirred at 70°C for 2 h. After cooling at room temperature, the
42 methanol was concentrated in a vacuum. This mixture was poured into 20 mL of saturated
43 Na₂CO₃ solution and extracted using EtOAc. The organic extracts were washed with water and
44 brine, subsequently dried over sodium sulfate, filtrated and concentrated under reduced pressure.
45 The title compound was obtained as a brown solid. Yield 0.71 g (79%); mp. 123 – 127 °C. ¹H
46 (200 MHz, DMSO-*d*₆) δ 7.48 (d, 2H, *J* = 8.0 Hz), 6.65 (d, 2H, *J* = 8.0 Hz), 4.86 (br s, 2H), 3.13
47
48
49
50
51
52
53
54
55
56
57
58
59
60

(s, 3H), 2.95 (s, 6H). ^{13}C NMR (50 MHz, DMSO- d_6) δ 169.4, 151.0, 130.1, 122.3, 110.4, 39.7.

The $-\text{NCH}_3$ signal likely has a chemical shift similar to the septet of DMSO- d_6 , making this effect difficult to view. IR (ATR, cm^{-1}): 3293, 3195, 2909, 2820, 1590. MS calculated for $\text{C}_{10}\text{H}_{15}\text{N}_3\text{O}$: $[\text{M}]^+ = 193.12$. Found: $[\text{M} + \text{H}]^+ = 193.99$.

General procedure for the preparation of methyl 3-(dimethoxymethyl)benzoate (**10a**) and methyl 4-(dimethoxymethyl)benzoate (**10b**).

A volume of 0.75 mL of 2,2-dimethoxypropane (6.39 mmol) and a catalytic amount of *p*-toluenesulfonic acid (0.074 g, 0.426 mmol) were added to a solution of aldehyde (**9a-9b**) (0.7 g, 4.26 mmol) in absolute methanol (10 mL). The resulting mixture was stirred at room temperature for 2 h, poured into 30 mL of saturated Na_2CO_3 solution and extracted using dichloromethane. The organic extracts were dried using sodium sulfate, filtrated and concentrated under reduced pressure.

Methyl 3-(dimethoxymethyl)benzoate (10a). The title intermediate was obtained at 85% yield as a colorless oil (0.85 g). ^1H NMR (200 MHz, DMSO- d_6) δ 7.98 (s, 1H), 7.94 (d, 1H, $J = 7.4$ Hz), 7.65 (d, 1H, $J = 7.4$ Hz), 7.54 (dd, 1H, $J = 7.4, 7.4$ Hz), 5.47 (s, 1H), 3.86 (s, 3H), 3.25 (s, 6H). ^{13}C NMR (50 MHz, DMSO- d_6) δ 166.2, 138.9, 131.3, 129.5, 129.1, 128.1, 127.1, 101.9, 52.6, 52.1. IR (ATR, cm^{-1}): 2952, 2831, 1720, 1097, 1050.

Methyl 4-(dimethoxymethyl)benzoate (10b). The title intermediate was obtained at 82% yield as a colorless oil (0.8 g). ^1H NMR (200 MHz, DMSO- d_6) δ 7.97 (d, 2H, $J = 8.2$ Hz), 7.52 (d, 2H,

1
2
3
4
5
6
7
8
9
10
11
12
13
14
15
16
17
18
19
20
21
22
23
24
25
26
27
28
29
30
31
32
33
34
35
36
37
38
39
40
41
42
43
44
45
46
47
48
49
50
51
52
53
54
55
56
57
58
59
60

$J = 8.2$ Hz), 5.46 (s, 1H), 3.86 (s, 3H), 3.25 (s, 6H). ^{13}C NMR (50 MHz, DMSO- d_6) δ 165.9, 143.2, 129.5, 129.0, 126.8, 101.9, 52.6, 52.1. IR (ATR, cm^{-1}): 2952, 2830, 1720, 1098, 1051.

General procedure for the preparation of 3-(dimethoxymethyl)-*N*-hydroxybenzamide (**11a**) and 4-(dimethoxymethyl)-*N*-hydroxybenzamide (**11b**).

Hydroxylamine hydrochloride (1.85 g, 26.65 mmol) was mixed in 15 mL of methanol with KOH (2.2 g, 39.96 mol) at room temperature, subsequently cooled to 0 °C, and filtrated, resulting in a basic solution of the hydroxylamine in methanol. In a round-bottom flask, the methyl ester (**10a-10b**) (0.7 g, 3.33 mol) was added to a basic hydroxylamine solution. The mixture was stirred at room temperature for 4 h. The methanol was concentrated in a vacuum, and 50 mL of distilled water was added to the round-bottom flask. The pH was adjusted to 7 using acetic acid. The resulting solution was extracted using EtOAc. The organic extracts were dried using sodium sulfate, filtered and concentrated under reduced pressure.

3-(Dimethoxymethyl)-*N*-hydroxybenzamide (11a). The title intermediate was obtained at 94% yield as a yellow oil (0.66 g). ^1H NMR (200 MHz, DMSO- d_6) δ 7.79 (s, 1H), 7.72 (d, 1H, $J = 7.2$ Hz), 7.48 – 7.41 (m, 2H), 5.41 (s, 1H), 3.25 (s, 6H). ^{13}C NMR (50 MHz, DMSO- d_6) δ 163.8, 138.5, 132.8, 129.1, 128.2, 126.7, 125.2, 101.9, 52.6. IR (ATR, cm^{-1}): 3202, 2830, 1633, 1040. MS calculated for $\text{C}_{18}\text{H}_{17}\text{N}_3\text{O}_3$: $[\text{M}]^- = 211.08$. Found: $[\text{M} - \text{H}]^- = 210.04$.

4-(Dimethoxymethyl)-*N*-hydroxybenzamide (11b). The title intermediate was obtained at 90% yield as a brown solid (0.63 g); mp. 73 – 77 °C. ^1H NMR (200 MHz, DMSO- d_6) δ 7.76 (d, 2H, $J = 8.1$ Hz), 7.44 (d, 2H, $J = 8.1$ Hz), 5.42 (s, 1H), 3.24 (s, 6H). ^{13}C NMR (50 MHz, DMSO- d_6) δ

1
2
3 163.8, 141.0, 132.8, 126.8, 126.5, 102.2, 52.5. IR (ATR, cm^{-1}): 3216, 2830, 1612, 1051. MS
4
5 calculated for $\text{C}_{18}\text{H}_{17}\text{N}_3\text{O}_3$: $[\text{M}]^- = 211.08$. Found: $[\text{M} - \text{H}]^- = 210.06$.
6
7
8
9

10 General procedure for the preparation of 3-formyl-*N*-hydroxybenzamide (**12a**) and 4-
11
12 formyl-*N*-hydroxybenzamide (**12b**).
13
14

15 A total of 10 mL of a 15% sulfuric acid solution in water (w/v) was added to a solution of
16
17 dimethyl acetal (**11a-11b**) (0.6 g, 2.84 mmol) in acetone (10 mL). The resulting mixture was
18
19 stirred at room temperature for 2 h, poured into 20 mL of water and extracted using EtOAc. The
20
21 organic extracts were dried using sodium sulfate, filtered and concentrated under reduced
22
23 pressure.
24
25
26
27
28

29 **3-Formyl-*N*-hydroxybenzamide (12a)**. The title intermediate was obtained at 87% yield as a
30
31 white solid (0.4 g); mp. 192 °C. ^1H NMR (400 MHz, $\text{DMSO}-d_6$) δ 11.45 (br s, 1H), 10.06 (s,
32
33 1H), 9.20 (br s, 1H), 8.29 (s, 1H), 8.07-8.05 (m, 2H), 7.69 (dd, 1H, $J = 7.9, 7.9\text{Hz}$). ^{13}C NMR (50
34
35 MHz, $\text{DMSO}-d_6$) δ 193.3, 163.7, 136.7, 134.2, 133.0, 132.4, 129.9, 128.4. IR (ATR, cm^{-1}): 3299,
36
37 3058, 1682, 1602. MS calculated for $\text{C}_8\text{H}_7\text{NO}_3$: $[\text{M}]^+ = 165.04$. Found: $[\text{M} + \text{H}]^+ = 166.05$.
38
39
40
41
42

43 **4-Formyl-*N*-hydroxybenzamide (12b)**. The title intermediate was obtained at 91% yield as
44
45 white solid (0.46 g); mp. 200 °C. ^1H NMR (400 MHz, $\text{DMSO}-d_6$) δ 11.46 (br s, 1H), 10.06 (s,
46
47 1H), 7.98 (d, 2H, $J = 8.0\text{ Hz}$), 7.91 (d, 2H, $J = 8.0\text{ Hz}$). ^{13}C NMR (50 MHz, $\text{DMSO}-d_6$) δ 193.3,
48
49 163.7, 138.4, 138.3, 130.0, 128.1. IR (ATR, cm^{-1}): 3291, 2741, 1687, 1606. MS calculated for
50
51 $\text{C}_8\text{H}_7\text{NO}_3$: $[\text{M}]^+ = 165.04$. Found: $[\text{M} + \text{H}]^+ = 165.98$.
52
53
54
55
56
57
58
59
60

1
2
3 **General procedure for the preparation of NAH series.** To a solution of **6a** or **6b** (1.67 mmol)
4
5 in absolute ethanol (7 mL) containing one drop of 37% hydrochloric acid, 1.67 mmol of the
6
7 corresponding aromatic aldehyde derivative was added. The mixture was stirred at room
8
9 temperature for 2 h until extensive precipitation was observed. The solvent was then partially
10
11 concentrated at reduced pressure, and the precipitate was filtered, washed with hexane and dried
12
13 under a vacuum to obtain the desired NAH derivatives.
14
15
16
17
18
19

20 **(E)-3-((2-(4-(Dimethylamino)benzoyl)hydrazono)methyl)benzoic acid (2a).** The title
21
22 compound was obtained as a yellow powder at 93% yield after condensation of **6a** using 3-
23
24 formylbenzoic acid; mp. 283 °C. ¹H NMR (500 MHz, DMSO-*d*₆) δ 11.66 (br s, 1H), 8.49 (br s,
25
26 1H), 8.31 (s, 1H), 7.98 (d, 1H, *J* = 7.7 Hz), 7.92 (d, 1H, *J* = 7.7 Hz), 7.84 (d, 2H, *J* = 8.6 Hz),
27
28 7.59 (dd, 1H, *J* = 7.7, 7.7 Hz), 6.77 (d, 2H, *J* = 8.6 Hz), 3.01 (s, 6H). ¹³C NMR (125 MHz,
29
30 DMSO-*d*₆) δ 167.3, 163.4, 152.9, 145.4, 135.5, 131.6, 131.1, 130.5, 129.6, 129.5, 127.5, 119.6,
31
32 111.2, 40.0. IR (ATR, cm⁻¹): 3333, 2909, 1700, 1592, 1521. LRMS calculated for C₁₇H₁₇N₃O₃:
33
34 [M]⁺ = 311.13. Found: [M + H]⁺ = 312.17. HRMS calculated for C₁₇H₁₇N₃O₃Na: [M+Na]⁺ =
35
36 334.1162. Found = 334.1160. 99.35% purity in HPLC, *t*_r = 4.33 min (λ = 335 nm).
37
38
39
40
41
42

43 **Methyl (E)-3-((2-(4-(dimethylamino)benzoyl)hydrazono)methyl)benzoate (2b).** The title
44
45 compound was obtained as a yellow powder at 89% yield after condensation of **6a** with **9a**; mp.
46
47 193 °C. ¹H NMR (400 MHz, DMSO-*d*₆) δ 11.68 (br s, 1H), 8.49 (br s, 1H), 8.34 (s, 1H), 7.98 (d,
48
49 1H, *J* = 7.8 Hz), 7.94 (d, 1H, *J* = 7.8 Hz), 7.84 (d, 2H, *J* = 8.6 Hz), 7.61 (dd, 1H, *J* = 7.8, 7.8 Hz),
50
51 6.77 (d, 2H, *J* = 8.6 Hz), 3.91 (s, 3H), 3.01 (s, 6H). ¹³C NMR (100 MHz, DMSO-*d*₆) δ 166.2,
52
53 163.3, 152.8, 145.1, 135.6, 132.1, 130.4, 129.7, 129.7, 129.5, 127.0, 119.5, 111.1, 52.6, 39.9. IR
54
55
56
57
58
59
60

(ATR, cm^{-1}): 3351, 2904, 1714, 1603, 1525. LRMS calculated for $\text{C}_{18}\text{H}_{19}\text{N}_3\text{O}_3$: $[\text{M}]^+ = 325.14$. Found: $[\text{M} + \text{H}]^+ = 326.21$. HRMS calculated for $\text{C}_{18}\text{H}_{19}\text{N}_3\text{O}_3\text{Na}$: $[\text{M} + \text{Na}]^+ = 348.1318$. Found = 348.1319. 97.88% purity in HPLC, $t_r = 8.51$ min ($\lambda = 341$ nm).

(E)-3-((2-(4-(Dimethylamino)benzoyl)hydrazono)methyl)-N-hydroxybenzamide (2c). The title compound was obtained as a yellow powder at 82% yield after condensation of **6a** with **12a**; mp. 216 °C. ^1H NMR (400 MHz, $\text{DMSO}-d_6$) δ 11.72 (br s, 1H), 8.50 (br s, 1H), 8.11 (s, 1H), 7.87 (d, 2H, $J = 8.7$ Hz), 7.84 (d, 1H, $J = 7.9$ Hz), 7.78 (d, 1H, $J = 7.9$ Hz), 7.54 (dd, 1H, $J = 7.9$, 7.9 Hz), 6.81 (d, 2H, $J = 8.7$ Hz), 3.01 (s, 6H). ^{13}C NMR (100 MHz, $\text{DMSO}-d_6$) δ 164.1, 163.3, 152.6, 145.7, 135.2, 133.7, 129.7, 129.4, 129.4, 128.2, 125.6, 120.0, 111.5, 40.2. IR (ATR, cm^{-1}): 3183, 1656, 1600, 1520. LRMS calculated for $\text{C}_{17}\text{H}_{18}\text{N}_4\text{O}_3$: $[\text{M}]^+ = 326.14$. Found: $[\text{M} + \text{H}]^+ = 327.20$. HRMS calculated for $\text{C}_{17}\text{H}_{18}\text{N}_4\text{O}_3\text{Na}$: $[\text{M} + \text{Na}]^+ = 349.1271$. Found = 349.1279. 97.63% purity in HPLC, $t_r = 3.48$ min ($\lambda = 341$ nm).

(E)-3-((2-(4-(Dimethylamino)benzoyl)-2-methylhydrazono)methyl)benzoic acid (2d). The title compound was obtained as a white powder at 75% yield after condensation of **6b** with 3-formylbenzoic acid; mp. 213 °C. ^1H NMR (400 MHz, $\text{DMSO}-d_6$) δ 8.23 (s, 1H), 8.07 (br s, 1H), 7.92 (d, 1H, $J = 7.8$ Hz), 7.81 (d, 1H, $J = 7.8$ Hz), 7.70 (d, 2H, $J = 8.9$ Hz), 7.54 (dd, 1H, $J = 7.8$, 7.8 Hz), 6.87 (d, 2H, $J = 8.9$ Hz), 3.48 (s, 3H), 3.03 (s, 6H). ^{13}C NMR (100 MHz, $\text{DMSO}-d_6$) δ 169.6, 167.3, 151.0, 138.9, 135.9, 132.3, 131.5, 131.0, 130.1, 129.5, 128.1, 123.0, 111.6, 40.7, 29.3. IR (ATR, cm^{-1}): 2551, 1687, 1644, 1592. LRMS calculated for $\text{C}_{18}\text{H}_{19}\text{N}_3\text{O}_3$: $[\text{M}]^+ = 325.14$. Found: $[\text{M} + \text{H}]^+ = 326.19$. HRMS calculated for $\text{C}_{18}\text{H}_{19}\text{N}_3\text{O}_3\text{Na}$: $[\text{M} + \text{Na}]^+ = 348.1318$. Found = 348.1318. 99.17% purity in HPLC, $t_r = 12.03$ min ($\lambda = 281$ nm).

Methyl (*E*)-3-((2-(4-(dimethylamino)benzoyl)-2-methylhydrazono)methyl)benzoate (2e**).**

The title compound was obtained as a white powder at 98% yield after condensation of **6b** with **9a**; mp. 108 °C. ¹H NMR (500 MHz, DMSO-*d*₆) δ (ppm): 8.25 (dd, 1H, *J* = 1.8, 1.6 Hz), 8.07 (s, 1H), 7.92 (ddd, 1H, *J* = 7.9, 1.8, 1.6 Hz), 7.84 (ddd, 1H, *J* = 7.9, 1.8, 1.6 Hz), 7.68 (dd, 2H, *J* = 9.0, 2.0 Hz), 7.56 (dd, 1H, *J* = 7.9, 7.9 Hz), 6.73 (dd, 2H, *J* = 9.0 Hz, 2.0 Hz), 3.87 (s, 3H), 3.47 (s, 3H), 3.01 (s, 6H). ¹³C NMR (125 MHz, DMSO-*d*₆) δ 169.5, 166.2, 152.0, 138.4, 136.3, 132.5, 131.4, 130.3, 129.7, 129.6, 127.9, 121.2, 110.3, 52.5, 40.0, 29.2. IR (ATR, cm⁻¹): 2945, 1711, 1630, 1598. LRMS calculated for C₁₉H₂₁N₃O₃: [M]⁺ = 339.16. Found: [M + H]⁺ = 340.21. HRMS calculated for C₁₉H₂₁N₃O₃Na: [M+Na]⁺ = 362.1475 Found = 362.1447. 98.96% purity in HPLC, t_r = 26.48 min (λ = 291 nm).

(*E*)-3-((2-(4-(Dimethylamino)benzoyl)-2-methylhydrazono)methyl)-*N*-hydroxybenzamide

(2f). The title compound was obtained as a white powder at 83% yield after condensation of **6b** with **12a**; mp. 197 °C. ¹H NMR (400 MHz, DMSO-*d*₆) δ 8.05 (s, 1H), 8.00 (br, 1H), 7.73 – 7.69 (m, 4H), 7.47 (dd, 1H, *J* = 7.8, 7.7 Hz), 6.98 (d, 2H, *J* = 7.8 Hz), 3.49 (s, 3H), 3.05 (s, 6H). ¹³C NMR (100 MHz, DMSO-*d*₆) δ 169.5, 164.3, 150.4, 139.3, 135.6, 133.7, 132.2, 129.2, 129.2, 127.5, 126.4, 124.5, 112.5, 41.2, 29.3. IR (ATR, cm⁻¹): 3170, 1650, 1635, 1589. LRMS calculated for C₁₈H₂₀N₄O₃: [M]⁺ = 340.15. Found: [M + H]⁺ = 341.20. HRMS calculated for C₁₈H₂₀N₄O₃Na: [M+Na]⁺ = 363.1427. Found = 363.1409. 98.58% purity in HPLC, t_r = 4.31 min (λ = 281 nm).

1
2
3 **(E)-4-((2-(4-(Dimethylamino)benzoyl)hydrazono)methyl)benzoic acid (3a).** The title
4
5 compound was obtained as a yellow powder at 62% yield after condensation of **6a** with 4-
6
7 formylbenzoic acid; mp. >300 °C. ¹H NMR (400 MHz, DMSO-*d*₆) δ 11.80 (br s, 1H), 8.54 (br s,
8
9 1H), 8.00 (d, 2H, *J* = 8.2 Hz), 7.86 (d, 2H, *J* = 8.7 Hz), 7.81 (d, 2H, *J* = 8.2 Hz), 6.76 (d, 2H, *J* =
10
11 8.7 Hz), 3.01 (s, 6H). ¹³C NMR (100 MHz, DMSO-*d*₆) δ 167.3, 163.4, 152.8, 145.3, 139.6,
12
13 131.7, 130.1, 129.4, 127.2, 119.5, 111.2, 40.1. IR (ATR, cm⁻¹): 3224, 1698, 1672, 1536. LRMS
14
15 calculated for C₁₇H₁₇N₃O₃: [M]⁺ = 311.13. Found: [M + H]⁺ = 312.17. LRMS calculated for
16
17 C₁₇H₁₇N₃O₃Na: [M+Na]⁺ = 334.1162. Found = 334.1159. 98.53% purity in HPLC, t_r = 4.27 min
18
19 (λ = 348 nm).
20
21
22
23
24
25
26

27 **Methyl (E)-4-((2-(4-(dimethylamino)benzoyl)hydrazono)methyl)benzoate (3b).** The title
28
29 compound was obtained as a yellow powder at 83% yield after condensation of **6a** with **9b**; mp.
30
31 255 °C. ¹H NMR (400 MHz, DMSO-*d*₆) δ 11.84 (br s, 1H), 8.52 (br s, 1H), 8.03 (d, 2H, *J* = 8.4
32
33 Hz), 7.87 (d, 2H, *J* = 8.9 Hz), 7.84 (d, 2H, *J* = 8.4 Hz), 6.83 (d, 2H, *J* = 8.9 Hz), 3.88 (s, 3H),
34
35 3.02 (s, 6H). ¹³C NMR (100 MHz, DMSO-*d*₆) δ 166.2, 163.3, 152.4, 145.1, 139.5, 130.2, 130.0,
36
37 129.7, 127.3, 120.2, 111.7, 52.5, 40.3. IR (ATR, cm⁻¹): 3307, 1692, 1660, 1599. LRMS
38
39 calculated for C₁₈H₁₉N₃O₃: [M]⁺ = 325.14. Found: [M + H]⁺ = 326.20. HRMS calculated for
40
41 C₁₈H₁₉N₃O₃Na: [M+Na]⁺ = 348.1318. Found = 348.1321. 99.25% purity in HPLC, t_r = 8.28 min
42
43
44
45
46 (λ = 348 nm).
47
48
49
50

51 **(E)-4-((2-(4-(Dimethylamino)benzoyl)hydrazono)methyl)-N-hydroxybenzamide (3c).** The
52
53 title compound was obtained as a yellow powder at 84% yield after condensation of **6a** with **12b**;
54
55 mp. 260 °C. ¹H NMR (400 MHz, DMSO-*d*₆) δ 11.67 (br s, 1H), 11.32 (br s, 1H), 8.47 (br s, 1H),
56
57
58
59
60

1
2
3 7.84 (d, 2H, $J = 8.5$ Hz), 7.83 (d, 2H, $J = 7.7$ Hz), 7.78 (d, 2H, $J = 7.7$ Hz), 6.77 (d, 2H, $J = 8.5$
4 Hz), 3.00 (s, 6H). ^{13}C NMR (100 MHz, DMSO- d_6) δ 164.1, 163.4, 152.9, 145.5, 137.7, 134.0,
5
6 129.6, 127.7, 127.1, 119.6, 111.2, 40.0. IR (ATR, cm^{-1}): 3234, 1643, 1599, 1520. LRMS
7
8 calculated for $\text{C}_{17}\text{H}_{18}\text{N}_4\text{O}_3$: $[\text{M}]^+ = 326.14$. Found: $[\text{M} + \text{H}]^+ = 327.20$. HRMS calculated for
9
10 $\text{C}_{17}\text{H}_{18}\text{N}_4\text{O}_3\text{Na}$: $[\text{M} + \text{Na}]^+ = 349.1271$. Found = 349.1270. 99.43% purity in HPLC, $t_r = 3.22$ min
11
12
13
14
15 ($\lambda = 344$ nm).
16
17
18
19

20 **(E)-4-((2-(4-(Dimethylamino)benzoyl)-2-methylhydrazono)methyl)benzoic acid (3d).** The
21
22 title compound was obtained as a white powder at 86% yield after condensation of **6b** with 4-
23
24 formylbenzoic acid; mp. >300 °C. ^1H NMR (400 MHz, DMSO- d_6) δ 8.03 (br s, 1H), 7.97 (d, 2H,
25
26 $J = 8.3$ Hz), 7.71 (d, 2H, $J = 8.3$ Hz), 7.67 (d, 2H, $J = 8.9$ Hz), 6.74 (d, 2H, $J = 8.9$ Hz), 3.48 (s,
27
28 3H), 3.01 (s, 6H). ^{13}C NMR (100 MHz, DMSO- d_6) δ 169.6, 167.2, 152.0, 139.6, 138.5, 132.5,
29
30 131.1, 129.6, 127.1, 120.8, 110.3, 39.9, 29.5. IR (ATR, cm^{-1}): 3075, 1705, 1610, 1590. LRMS
31
32 calculated for $\text{C}_{18}\text{H}_{19}\text{N}_3\text{O}_3$: $[\text{M}]^+ = 325.14$. Found: $[\text{M} + \text{H}]^+ = 326.20$. HRMS calculated for
33
34 $\text{C}_{18}\text{H}_{19}\text{N}_3\text{O}_3\text{Na}$: $[\text{M} + \text{Na}]^+ = 348.1318$. Found = 348.1319. 96.52% purity in HPLC, $t_r = 12.19$ min
35
36
37
38
39
40
41
42
43
44
45
46
47
48
49
50
51
52
53
54
55
56
57
58
59
60

Methyl (E)-4-((2-(4-(dimethylamino)benzoyl)-2-methylhydrazono)methyl)benzoate (3e).

The title compound was obtained as a white powder at 88% yield after condensation of **6b** with
9b; mp. 156 °C. ^1H NMR (400 MHz, DMSO- d_6) δ 8.04 (s, 1H), 7.98 (d, 2H, $J = 8.3$ Hz), 7.72 (d,
2H, $J = 8.3$ Hz), 7.67 (d, 2H, $J = 8.9$ Hz), 6.73 (d, 2H, $J = 8.9$ Hz), 3.88 (s, 3H), 3.48 (s, 3H),
3.01 (s, 6H). ^{13}C NMR (100 MHz, DMSO- d_6) δ 169.6, 166.2, 152.1, 140.1, 138.4, 132.5, 130.1,
129.2, 127.2, 120.7, 110.4, 52.4, 39.9, 29.5. IR (ATR, cm^{-1}): 2903, 1716, 1644, 1599. LRMS

1
2
3 calculated for $C_{19}H_{21}N_3O_3$: $[M]^+ = 339.16$. Found: $[M + H]^+ = 340.21$. HRMS calculated for
4
5 $C_{19}H_{21}N_3O_3Na$: $[M+Na]^+ = 362.1475$. Found = 362.1472. 97.73% purity in HPLC, $t_r = 17.74$ min
6
7
8 ($\lambda = 297$ nm).
9

10
11
12 **(E)-4-((2-(4-(Dimethylamino)benzoyl)-2-methylhydrazono)methyl)-N-hydroxybenzamide**

13 **(3f)**. The title compound was obtained as a white powder at 75% yield after condensation of **6b**
14
15 with **12b**; mp. 213 °C. 1H NMR (400 MHz, DMSO- d_6) δ 8.05 (s, 1H), 7.79 (d, 2H, $J = 8.2$ Hz),
16
17 7.72 (d, 2H, $J = 8.7$ Hz), 7.63 (d, 2H, $J = 8.2$ Hz), 7.12 (d, 2H, $J = 8.7$ Hz), 3.49 (s, 3H), 3.07 (s,
18
19 6H). ^{13}C NMR (100 MHz, DMSO- d_6) δ 169.4, 163.9, 149.4, 139.3, 137.8, 133.2, 132.0, 127.4,
20
21 127.0, 126.4, 113.9, 41.9, 29.3. IR (ATR, cm^{-1}): 2963, 2809, 1631, 1591. LRMS calculated for
22
23 $C_{18}H_{20}N_4O_3$: $[M]^+ = 340.15$. Found: $[M + H]^+ = 341.20$. HRMS calculated for $C_{18}H_{20}N_4O_3Na$:
24
25 $[M+Na]^+ = 363.1427$. Found = 363.1425. 97.17% purity in HPLC, $t_r = 4.16$ min ($\lambda = 292$ nm).
26
27
28
29
30
31
32
33

34 **4-Acetyl-N-hydroxybenzamide (14)**. 4-Acetylbenzoic acid (**13**) (0.1 g, 0.61 mmol) and one
35
36 drop of DMF were dissolved in CH_2Cl_2 (20 mL), and 0.105 mL of oxalyl chloride (1.22 mmol)
37
38 was slowly added. Vigorous gas evolution was observed. After stirring for 2 h, this solution was
39
40 slowly added to a solution of hydroxylamine (50 wt % in water, 0.056 mL, 0.61 mmol) and
41
42 triethylamine (0.25 mL, 1.83 mmol) in THF (20 mL) at 0 °C. After stirring for additional 30 min
43
44 at 0 °C, the solvent was concentrated in a vacuum. The mixture was poured into an aqueous
45
46 solution of 10% (w/v) NaOH and extracted using CH_2Cl_2 . The pH of the resulting water solution
47
48 was adjusted to 7 using an aqueous solution of 10% (w/v) HCl and extracted using EtOAc. The
49
50 organic phase was dried over Na_2SO_4 and evaporated in a vacuum. The residue was
51
52 recrystallized from aqueous ethanol: yield 0.07 g (64%); mp. 198 °C. 1H NMR (300 MHz,
53
54
55
56
57
58
59
60

1
2
3 DMSO-*d*₆) δ 11.39 (br s, 1H), 9.19 (br s, 1H); 8.01 (d, 2H, *J* = 8.4 Hz), 7.87 (d, 2H, *J* = 8.4 Hz),
4
5 2.61 (s, 3H). ¹³C NMR (75 MHz, DMSO-*d*₆) δ 198.0, 163.6, 138.8, 136.7, 128.4, 127.4, 27.10.
6
7
8 IR (ATR, cm⁻¹): 3293, 2742, 1680, 1268. MS calculated for C₉H₉NO₃: [M]⁻ = 179.06 Found: [M
9
10 - H]⁻ = 178.18.
11
12
13

14
15 **(*E*)-4-(1-(2-(4-(Dimethylamino)benzoyl)hydrazono)ethyl)-*N*-hydroxybenzamide (3g).** In a
16
17 microwave flask (Monowave 300; G30 type), **6a** (0.2 g, 1.116 mmol), **14** (0.2 g, 1.116 mmol),
18
19 10 mL of ethanol and one drop of acetic acid, which was used as the catalyst, were added. The
20
21 Monowave 300 microwave was programmed to reach 80 °C in 2 min, and the reaction was
22
23 maintained under microwave irradiation for 30 min at 80 °C. Extensive precipitation was
24
25 observed, and the white solid was filtered under a vacuum. The residue was recrystallized from
26
27 hot ethanol: yield 0.17 g (45%); mp. 222 – 223 °C. ¹H NMR (400 MHz, DMSO-*d*₆) δ 11.32 (br
28
29 s, 1H), 10.45 (br s, 1H), 9.09 (br s, 1H), 7.89 (d, 2H, *J* = 8.4 Hz), 7.81 (d, 2H, *J* = 8.9 Hz), 7.81
30
31 (d, 2H, *J* = 8.4 Hz), 6.75 (d, 2H, *J* = 8.9 Hz), 3.00 (s, 6H), 2.38 (s, 3H). ¹³C NMR (100 MHz,
32
33 DMSO-*d*₆) δ 164.5, 164.0, 152.7, 151.9, 141.1, 133.2, 130.1, 127.0, 126.4, 120.7, 111.0, 40.0,
34
35 14.3. IR (ATR, cm⁻¹): 3288, 1647, 1633, 1606, 1490, 1282, 1196, 821. LRMS calculated for
36
37 C₁₈H₂₀N₄O₃: [M]⁻ = 340.15 Found: [M - H]⁻ = 339.04. HRMS calculated for C₁₈H₂₀N₄O₃Na:
38
39 [M+Na]⁺ = 363.1427 Found = 363.1426. 97.21% purity in HPLC, *t*_r = 3.55 min (λ = 335 nm).
40
41
42
43
44
45
46
47

48 **(*E*)-4-(1-(2-(4-(Dimethylamino)benzoyl)-2-methylhydrazono)ethyl)-*N*-hydroxybenzamide**
49
50 **(3h).** In a microwave flask (Monowave 300) G30 type, **6b** (0.215 g, 1.116 mmol), **14** (0.2 g,
51
52 1.116 mmol), 10 mL of ethanol and one drop of acetic acid, which was used as a catalyst, were
53
54 added. The microwave Monowave 300 was programmed to reach 125 °C in 2 min, and the
55
56
57
58
59
60

1
2
3 reaction was maintained under microwave irradiation for 2 h at 125 °C. Under this condition, the
4
5 pressure inside the flask was 6 bar. The mixture was concentrated under a vacuum. The residue
6
7 was washed using EtOAc and recrystallized from hot ethanol: yield 0.15 g (35%); mp. 181 – 183
8
9 °C. ¹H NMR (400 MHz, DMSO-*d*₆) δ 11.32 (br s, 1H), 9.13 (br s, 1H), 7.87 (d, 2H, *J* = 8.5 Hz),
10
11 7.80 (d, 2H, *J* = 8.5 Hz), 7.41 (d, 2H, *J* = 8.9 Hz), 6.64 (d, 2H, *J* = 8.9 Hz), 3.27 (s, 3H), 2.94 (s,
12
13 6H), 2.31 (s, 3H). ¹³C NMR (100 MHz, DMSO-*d*₆) δ 169.1, 167.2, 163.8, 151.9, 139.8, 134.5,
14
15 130.7, 127.2, 127.2, 121.7, 110.7, 39.9, 17.2. The -NCH₃ signal likely has a chemical shift
16
17 similar to the septet of DMSO-*d*₆, making this effect difficult to view. IR (ATR, cm⁻¹): 3176,
18
19 1650, 1598, 1354, 1160, 1010, 836. LRMS calculated for C₁₉H₂₂N₄O₃: [M]⁻ = 354.17 Found: [M
20
21 - H]⁻ = 353.05. HRMS calculated for C₁₉H₂₂N₄O₃: [M+Na]⁺ = 377.1584. Found = 377.1587.
22
23 95.68% purity in HPLC, t_r = 3.54 min (λ = 293 nm).
24
25
26
27
28
29
30
31

32 **Solubility experiment.** The solubility experiment was based on ultraviolet absorbance.^{36,37} The
33
34 saturated aqueous solution (buffer 7.4) was stirred for 24 h, and the sample was filtered through a
35
36 0.45 μm filter and transferred to a quartz cuvette (10-mm optical path) to perform the reading.
37
38 The solubility was determined through linear regression using graph plots and solutions prepared
39
40 by dilutions of the original solution in methanol. The data were obtained in triplicate, and the
41
42 mean values were used to plot the graphs. The correlation coefficient (*R*²) values were between
43
44 0.996 and 0.999.
45
46
47

48 The log*D*_{7.4} values were determined from the saturated solutions obtained in the solubility
49
50 experiment. A total of 5 mL of saturated compound solution and 5 mL of n-octanol were added
51
52 to an Erlenmeyer flask, and the mixture was then stirred at 37 ° C for 4 h. The phases were
53
54 separated, and the aqueous phase was transferred to a quartz cuvette (10 mm optical path). The
55
56
57
58
59
60

1
2
3 logD_{7.4} value was then determined through linear regression using graph plots and solutions
4
5 prepared by dilutions of the original solution in methanol.
6
7
8
9

10 **Chemical stability study.** Two microliters (0.01 mmol) of a concentrated solution of the
11 compound under examination (40 mM stock solution solubilized in DMSO) and 248 μ L of acid
12 (0.2 M potassium chloride and 0.2 M HCl; pH 2.0) or neutral (phosphate dibasic, pH 7.4) buffer
13 were added to a 2-mL Eppendorf microtube. After vortexing, the mixture was placed in a water
14 bath at 37 °C under vigorous stirring for 0, 30, 60, 120 and 240 min. After each reaction, 248 μ L
15 of basic buffer (phosphate buffer, pH 8.4) was added to neutralize the pH of the medium in the
16 experiments using acidic buffer. The compound was extracted using 1 mL of acetonitrile
17 followed by vigorous vortexing and freezing of the aqueous phase (-10 °C). The organic phase
18 was separated, filtered and analyzed using an HPLC-PDA (acetonitrile/water 1:1, 0.05% of
19 TFA).
20
21
22
23
24
25
26
27
28
29
30
31
32
33
34
35

36 **HDAC inhibition.** The inhibition of HDAC from rat liver and recombinant human HDAC1, 2, 6
37 and 8 was realized in CEREP-France (www.cerep.fr) under the following study numbers:
38
39 100016044 (June 17, 2014), 100018551 (November 13, 2014), 100022694 (June 15, 2015).
40
41
42
43

44 For assessment of inhibition of the enzymatic activity of HDACs, HDACs were obtained
45 from rat livers and incubated with the fluorogenic substrate at a concentration of 20 μ M for 60
46 min at 37 °C. The formation of fluorolysine was detected through fluorimetry. The compounds
47 were used at a concentration of 1 μ M, and the enzyme activity was measured and compared with
48 the enzyme activity of the control (absence of inhibitor). The results are expressed in terms of
49 percentages of enzyme activity. To determine their ability to inhibit rat liver HDACs, the
50
51
52
53
54
55
56
57
58
59
60

1
2
3 compounds were tested through a six-point enzyme assay with a three-fold serial dilution starting
4
5 from 3 μM for **2c** and 1 μM for **3c** and **3f**.
6
7

8 To assay the selectivity profile against human HDAC, human recombinant HDAC1, 2, 6
9
10 and 8 were incubated with the fluorogenic substrate at a concentration of 20, 20, 25 and 400 μM
11
12 at room temperature for 15, 15, 30 and 90 min,. The formation of fluorolysine was detected
13
14 through fluorimetry. For determination of the IC_{50} , the compounds were tested through a seven-
15
16 point enzyme assay with a three-fold serial dilution starting from 10 μM for **2c** and **2f** and 3 μM
17
18 for **3c**, **3f**, **3h** and **3g**. The values are presented as the averages of three experiments.
19
20
21

22 The analysis was performed using software developed at Cerep (Hill software) and
23
24 GraphPad Prism® 5.0 (GraphPad Software, Inc., San Diego, CA, USA) and validated through
25
26 comparison with results generated using the SigmaPlot 4.0 software.
27
28
29
30
31

32 **Cell lines and culture conditions.** A549 (human lung carcinoma), MCF-7 (human breast
33
34 adenocarcinoma), HepG2 (human hepatocellular carcinoma), and HT-144 (melanoma) cell lines
35
36 were used in the present study. The cell cultures were maintained in DMEM (Dulbecco's
37
38 Modified Eagle's Medium, Sigma, CA, USA)/ F12 (Sigma) supplemented with 10% fetal bovine
39
40 serum (FBS, Cultilab, Sao Paulo, Brazil). The cells were grown in a 37°C humidified incubator
41
42 containing 5% CO_2 .
43
44
45
46
47

48 **Cell viability.** The cell viability was evaluated through a MTS assay according to Cory et al.
49
50 (1991) using a Promega non-radioactive cell proliferation assay.⁶⁴ The cells were plated onto 96-
51
52 wells at a density of 1×10^4 cells/well. After attachment (24 h), the cells were treated with
53
54 HDAC inhibitors for 48 h. This assay measures the amount of formazan produced from 3-(4,5-
55
56
57
58
59
60

1
2
3 dimethylthiazol-2-yl)-5-(3-carboxymethoxyphenyl)-2-(4-sulfophenyl)-2*H*-tetrazolium inner salt
4
5 (MTS) through the dehydrogenase enzymes of metabolically active cells. Thus, the quantity of
6
7 formazan produced (as measured by the absorbance at 490 nm) is directly proportional to the
8
9 number of living cells. The absorbance values of the treated cells were compared with the
10
11 absorbance values of untreated cells. The experiments were conducted in triplicate wells and
12
13 repeated three times. Means \pm standard deviations (SD) were calculated. The IC₅₀ value was
14
15 determined through non-linear regression using GraphPad Prism® 5.0 (GraphPad Software, Inc.,
16
17 San Diego, CA, USA).

21
22
23
24 **Cell cycle analysis.** Cell cycle analysis was performed according to Zanin et al. (2015).⁶⁵

25
26 Briefly, the cells were treated with compounds **3c** and **3g** at concentrations of 5 or 10 μ M for 24
27
28 and 48 h. The cells were fixed in 75% methanol overnight at 4°C. After washing twice with cold
29
30 PBS (phosphate-buffered saline), the cells were resuspended in dye solution [phosphate-buffered
31
32 saline (PBS) containing 30 μ g/mL propidium iodide (PI) and 3 mg/mL RNase]. DNA was
33
34 quantified after 1 h of staining. The analysis was performed using a flow cytometer (Guava
35
36 easyCyte 8HT, Hayward, CA, USA). The experiments were conducted in triplicate, and the data
37
38 are presented as the means \pm SD.

39
40
41
42
43
44
45 **TUNEL assay.** A total of 1×10^5 cells were seeded onto 24-well plates and incubated overnight
46
47 at 37°C prior to the addition of compound **3g** at the appropriate concentrations. After 24 h of
48
49 treatment, the cells were collected through enzymatic digestion and transferred to Falcon tubes.
50
51 After centrifugation (5 min at 1000 rpm), the pellets were homogenized in PBS, and the cells
52
53 were fixed with 4% paraformaldehyde for 30 min. After centrifugation, the pellets were re-
54
55
56
57
58
59
60

1
2
3 suspended in cold 70% ethanol and stored at -20 °C for at least 2 h. After fixation, the cells were
4
5 stained according to the protocol for the TUNEL assay (Guava Technologies, Hayward, CA,
6
7 USA). The cells were analyzed using a flow cytometer (easyCyte 8HT, Guava Technologies).
8
9 Positive and negative controls were used in each assay. The experiments were performed in
10
11 triplicate, and the results are presented as the means \pm SD.
12
13
14
15
16

17 **Caspase 3/7 activation.** Apoptosis onset was determined after assaying the intracellular
18
19 activation of caspase-3/7 using the Guava Caspase-3/7 FAM kit (Guava Technologies). The cells
20
21 were collected after 24 h of treatment with compound **3g** and re-suspended in warm PBS, and the
22
23 concentration was adjusted to 5×10^5 cells/ml. A volume of 100 μ L of each sample was incubated
24
25 with 10 μ L of caspase-3/7 carboxyfluorescein (FAM) reagent in U-bottomed 96-well plates at
26
27 37°C in a 5% CO₂ humidified incubator for 1 h. After incubation, the cells were washed and
28
29 subjected to 7-ADD viability staining. The analysis was performed using a flow cytometer
30
31 (Guava easyCyte 8HT, Hayward, CA, USA), and positive and negative controls were included in
32
33 the analysis. The experiments were performed in triplicate, and the results are presented as the
34
35 means \pm SD.
36
37
38
39
40
41
42

43 **Statistical analysis.** The quantitative data are presented as the means \pm SD from triplicates. The
44
45 statistical analysis was performed through analysis of variance (ANOVA) followed by the
46
47 Tukey's post-test. The GraphPad Prism® 5.0 (GraphPad Software, Inc., San Diego, CA, USA)
48
49 software was used, and differences were considered significant at $p < 0.05$.
50
51
52
53
54
55
56
57
58
59
60

1
2
3 **Western Blotting.** Briefly, the non-small cell lung cancer (NSCLC) cell lines A549 and Calu-1
4
5 were treated with either compound **3c** (15 and 30 nM) or **3f** (27 and 54 nM) or with DMSO
6
7 (control) for 24 h. The protein was extracted using lysis buffer from Invitrogen according to the
8
9 manufacturers' instructions, and 30 μ g of total protein was resolved through SDS-PAGE.
10
11 Acetylated tubulin was detected using an anti-acetyl antibody (Sigma-Aldrich), and anti-GAPDH
12
13 (Cell Signaling) was used as the loading control. The protein bands were visualized using an
14
15 ECL detection system.
16
17
18
19

20
21
22 **Scratch test.** The scratch test method was used to estimate cell migration. The cells were seeded
23
24 onto 12-well plates and treated with DMSO or compounds **3c** and **3f**. After tracing the bottom of
25
26 the wells, the cells were allowed to migrate. The images were captured after 48 h using an
27
28 Observer 2.1 microscope (Zeiss) with AxioCam HRc using a 10x objective and analyzed using
29
30 the ImageJ software.
31
32
33

34
35
36 **Molecular modeling.** All of the compounds were constructed and energy-minimized at the
37
38 HF/3-21G level using Spartan 08⁷ (Wavefunction Inc.; License Key:DQAIR, USB-HASP).
39

40
41 The HDAC8 crystallographic structures available in the PDB with codes 1VKG
42
43 (resolution: 2.20 Å)⁴² and 1W22 (resolution: 2.5 Å)⁴⁴ were used for docking runs with the GOLD
44
45 5.1 program (CCDC; License Key: G/414/2006). The four fitness functions available in the
46
47 program, namely ASP,⁶⁶ ChemPLP,⁶⁷ ChemScore^{68,69} and GoldScore,^{70,71} were evaluated for the
48
49 re-docking of the co-crystallized ligands to identify the most adequate fitness function for the
50
51 docking studies into HDAC8. Crystallographic water molecules were removed during the
52
53 docking runs, and the binding site was determined within a distance of 15 Å from the zinc ion.
54
55
56
57
58
59
60

1
2
3 After docking, the RMSD between the best result for each fitness function and the
4
5
6 crystallographic structure was calculated.

7
8 The fitness function with the best performance in the re-docking test for HDAC8 was
9
10 ChemScore because the expected chelating interaction between the ligand's hydroxamic acid
11
12 moiety and the zinc ion in a bidentate pattern and the hydrogen bonds between the ligand and the
13
14 His142 and His143 residues were correctly predicted for this enzyme using this function.⁴²The
15
16 RMSDs were equal to 2.1 Å and 2.2 Å for the re-docking with 1VKG and 1W22, respectively,
17
18 and both of these values are below the resolution of the corresponding crystallographic structure.
19
20
21
22 ChemScore was thus used for the docking study of the compounds described in this study.

23
24 For HDAC6, the modeling was focused only on the second catalytic subunit (CDII,
25
26 Thr481-Gly800). Because no crystal structures are available for this enzyme, a model was
27
28 constructed with SWISS-MODEL Workspace⁴⁵⁻⁴⁷ using the crystallographic structure of a
29
30 HDAC7 isoenzyme with code 3C0Z (resolution: 2.1 Å),⁴⁸ which presents a sequence identity of
31
32 49.84% and a coverage of 0.99 with the target enzyme. To introduce the zinc ion into the
33
34 catalytic site of the modeled structure, the Cartesian coordinates were extracted from the same
35
36 crystallographic structure used as a template. To assess the quality of the model, we performed
37
38 an analysis of the Ramachandran plot generated through RAMPAGE.⁷² Only 2.5% of the amino
39
40 acid residues were in the outlier region, and none of these residues were involved in any
41
42 interaction with the ligands in the active site. The docking studies were run using the GOLD 5.1
43
44 program with the same fitness function used for HDAC8 (ChemScore). The pictures in Figure 5
45
46 were constructed with PyMOL 6.0 program.
47
48
49
50
51
52
53
54
55
56
57
58
59
60

ASSOCIATED CONTENT**§Supporting Information**

¹H NMR spectra of *meta* (**2a-2f**) and *para* analogs (**3a-3h**), NOEdiff experiment for **3c**, **3f** and **3g**, curves of determination of IC₅₀ of the compounds, HPLC of *meta* (**2a-2f**) and *para* analogs (**3a-3h**) and validation of the HDAC6 homology model. This material is available free of charge via the Internet at <http://pubs.acs.org>.

AUTHOR INFORMATION**Corresponding Author**

*Phone: +55-21-2562-6447. E-mail: cmfraga@ccsdecania.ufrj.br

Notes

The authors declare no competing financial interests.

ACKNOWLEDGMENTS

The authors would like to thank INCT-INOVAR (BR, Grant No. 573.564/2008-6), Fundação do Câncer (BR), CNPq (BR), and FAPERJ (BR, Grants No. E-26/101.555/2014 and E-26/202.918/2015) for the financial support provided and the fellowships awarded. The authors would also like to thank MSc. Eduardo Miguez (Institute of Macromolecules, UFRJ) for the realization of the NOEdiff experiments.

ABBREVIATIONS USED

1
2
3 HDAC, histone deacetylase; NAH, *N*-acylhydrazone; HAT, histone acetyltransferases; HDACI,
4 HDAC inhibitors; CTCL, cutaneous T-cell lymphoma; PTCL, peripheral T-cell lymphoma;
5
6 SAR, structure-activity relationships; SAHA, suberoylanilide hydroxamic acid; ZBG, zinc-
7
8 binding group; IC₅₀, half-maximal inhibitory concentration; DMSO, dimethylsulfoxide; HCC,
9
10
11
12
13 hepatocellular carcinoma.
14
15
16
17
18
19
20
21
22
23
24
25
26
27
28
29
30
31
32
33
34
35
36
37
38
39
40
41
42
43
44
45
46
47
48
49
50
51
52
53
54
55
56
57
58
59
60

1
2
3
4
5
6
7
8
9
10
11
12
13
14
15
16
17
18
19
20
21
22
23
24
25
26
27
28
29
30
31
32
33
34
35
36
37
38
39
40
41
42
43
44
45
46
47
48
49
50
51
52
53
54
55
56
57
58
59
60
REFERENCES

- (1) Kouzarides, T. Chromatin modifications and their function. *Cell* **2007**, *128*, 693-705.
- (2) Glozak, M. A.; Seto, E. Histone deacetylases and cancer. *Oncogene* **2007**, *26*, 5420-5432.
- (3) Witt, O.; Deubzer, H. E.; Milde, T.; Oehme, I. HDAC family: what are the cancer relevant targets? *Cancer Lett.* **2009**, *277*, 8-21.
- (4) Gregoretto, I. V.; Lee, Y.-M.; Goodson, H. V. Molecular evolution of the histone deacetylase family: functional implications of phylogenetic analysis. *J. Mol. Biol.* **2004**, *338*, 17-31.
- (5) Dokmanovic, M.; Clarke, C.; Marks, P. A. Histone deacetylase inhibitors: overview and perspectives. *Mol. Cancer Res.* **2007**, *5*, 981-989.
- (6) Falkenberg, K. J.; Johnstone, R. W. Histone deacetylases and their inhibitors in cancer, neurological diseases and immune disorders. *Nat. Rev. Drug Discov.* **2014**, *13*, 673-691.
- (7) Bolden, J. E.; Peart, M. J.; Johnstone, R. W. Anticancer activities of histone deacetylase inhibitors. *Nat. Rev. Drug Discov.* **2006**, *5*, 769-784.
- (8) Liu, T.; Kuljaca, S.; Tee, A.; Marshall, G. M. Histone deacetylase inhibitors: multifunctional anticancer agents. *Cancer Treat. Rev.* **2006**, *32*, 157-165.
- (9) Marks, P. A.; Breslow, R. Dimethyl sulfoxide to vorinostat: development of this histone deacetylase inhibitor as an anticancer drug. *Nat. Biotechnol.* **2007**, *25*, 84-90.
- (10) Yang, L. P. Romidepsin: in the treatment of T-cell lymphoma. *Drugs* **2011**, *71*, 1469-1480.
- (11) Prince, H. M.; Dickinson, M. Romidepsin for cutaneous T-cell lymphoma. *Clin. Cancer Res.* **2012**, *18*, 3509-3515.
- (12) Poole, R. M. Belinostat: first global approval. *Drugs* **2014**, *74*, 1543-1554.

- 1
2
3 (13) Garnock-Jones, K. P. Panobinostat: first global approval. *Drugs* **2015**, *75*, 695-704.
4
5
6 (14) Miller, T. A.; Witter, D. J.; Belvedere, S. Histone deacetylase inhibitors. *J. Med. Chem.*
7
8 **2003**, *46*, 5097-5116.
9
10 (15) Thaler, F.; Mercurio, C. Towards selective inhibition of histone deacetylase isoforms:
11 what has been achieved, where we are and what will be next. *ChemMedChem* **2014**, *9*, 523-536.
12
13 (16) Kalin, J. H.; Bergman, J. A. Development and therapeutic implications of selective
14 histone deacetylase 6 inhibitors. *J. Med. Chem.* **2013**, *56*, 6297-6313.
15
16 (17) Suzuki, T.; Ota, Y.; Ri, M.; Bando, M.; Gotoh, A.; Itoh, Y.; Tsumoto, H.; Tatum, P. R.;
17 Mizukami, T.; Nakagawa, H.; Iida, S.; Ueda, R.; Shirahige, K.; Miyata, N. Rapid discovery of
18 highly potent and selective inhibitors of histone deacetylase 8 using click chemistry to generate
19 candidate libraries. *J. Med. Chem.* **2012**, *55*, 9562-9575.
20
21 (18) Chakrabarti, A.; Oehme, I.; Witt, O.; Oliveira, G.; Sippl, W.; Romier, C.; Pierce, R. J.;
22 Jung, M. HDAC8: a multifaceted target for therapeutic interventions. *Trends Pharmacol. Sci.*
23 **2015**, *36*, 481-492.
24
25 (19) Valenzuela-Fernandez, A.; Cabrero, J. R.; Serrador, J. M.; Sanchez-Madrid, F. HDAC6:
26 a key regulator of cytoskeleton, cell migration and cell-cell interactions. *Trends. Cell. Biol.* **2008**,
27 *18*, 291-297.
28
29 (20) Oehme, I.; Deubzer, H. E.; Wegener, D.; Pickert, D.; Linke, J. P.; Hero, B.; Kopp-
30 Schneider, A.; Westermann, F.; Ulrich, S. M.; von Deimling, A.; Fischer, M.; Witt, O. Histone
31 deacetylase 8 in neuroblastoma tumorigenesis. *Clin. Cancer Res.* **2009**, *15*, 91-99.
32
33 (21) Wu, J.; Du, C.; Lv, Z.; Ding, C.; Cheng, J.; Xie, H.; Zhou, L.; Zheng, S. The up-
34 regulation of histone deacetylase 8 promotes proliferation and inhibits apoptosis in
35 hepatocellular carcinoma. *Dig. Dis. Sci.* **2013**, *58*, 3545-3553.
36
37
38
39
40
41
42
43
44
45
46
47
48
49
50
51
52
53
54
55
56
57
58
59
60

1
2
3 (22) Park, S. Y.; Jun, J. A.; Jeong, K. J.; Heo, H. J.; Sohn, J. S.; Lee, H. Y.; Park, C. G.;
4
5 Kang, J. Histone deacetylase 1, 6 and 8 are critical for invasion in breast cancer. *Oncol. Rep.*
6
7 **2011**, *25*, 1677-1681.
8
9

10 (23) Olson, D. E.; Wagner, F. F.; Kaya, T.; Gale, J. P.; Aidoud, N.; Davoine, E. L.; Lazzaro,
11
12 F.; Weiwer, M.; Zhang, Y. L.; Holson, E. B. Discovery of the first histone deacetylase 6/8 dual
13
14 inhibitors. *J. Med. Chem.* **2013**, *56*, 4816-4820.
15
16

17 (24) Tang, G.; Wong, J. C.; Zhang, W.; Wang, Z.; Zhang, N.; Peng, Z.; Zhang, Z.; Rong, Y.;
18
19 Li, S.; Zhang, M.; Yu, L.; Feng, T.; Zhang, X.; Wu, X.; Wu, J. Z.; Chen, L. Identification of a
20
21 novel aminotetralin class of HDAC6 and HDAC8 selective inhibitors. *J. Med. Chem.* **2014**, *57*,
22
23 8026-8034.
24
25

26 (25) Finnin, M. S.; Donigian, J. R.; Cohen, A.; Richon, V. M.; Rifkind, R. A.; Marks, P. A.;
27
28 Breslow, R.; Pavletich, N. P. Structures of a histone deacetylase homologue bound to the TSA
29
30 and SAHA inhibitors. *Nature* **1999**, *401*, 188-193.
31
32

33 (26) Lima, L. M.; Barreiro, E. J. Bioisosterism: a useful strategy for molecular modification
34
35 and drug design. *Curr. Med. Chem.* **2005**, *12*, 23-49.
36
37

38 (27) Patani, G. A.; LaVoie, E. J. Bioisosterism: a rational approach in drug design. *Chem.*
39
40 *Rev.* **1996**, *96*, 3147-3176.
41
42

43 (28) Duarte, C. D.; Barreiro, E. J.; Fraga, C. A. Privileged structures: a useful concept for the
44
45 rational design of new lead drug candidates. *Mini-Rev. Med. Chem.* **2007**, *7*, 1108-1119.
46
47

48 (29) Barreiro, E. J.; Kummerle, A. E.; Fraga, C. A. The methylation effect in medicinal
49
50 chemistry. *Chem. Rev.* **2011**, *111*, 5215-5246.
51
52

53 (30) Kummerle, A. E.; Schmitt, M.; Cardozo, S. V.; Lugnier, C.; Villa, P.; Lopes, A. B.;
54
55 Romeiro, N. C.; Justiniano, H.; Martins, M. A.; Fraga, C. A.; Bourguignon, J. J.; Barreiro, E. J.
56
57
58
59
60

1
2
3 Design, synthesis, and pharmacological evaluation of N-acylhydrazones and novel
4
5 conformationally constrained compounds as selective and potent orally active
6
7 phosphodiesterase-4 inhibitors. *J. Med. Chem.* **2012**, *55*, 7525-7545.

8
9
10 (31) Tang, C.; Li, C.; Zhang, S.; Hu, Z.; Wu, J.; Dong, C.; Huang, J.; Zhou, H. B. Novel
11
12 bioactive hybrid compound dual targeting estrogen receptor and histone deacetylase for the
13
14 treatment of breast cancer. *J. Med. Chem.* **2015**, *58*, 4550-4572.

15
16
17 (32) Yamada, S.; Morizono, D.; Yamamoto, K. Mild oxidation of aldehydes to the
18
19 corresponding carboxylic acids and esters: alkaline iodine oxidation revisited. *Tetrahedron Lett.*
20
21 **1992**, *33*, 4329-4332.

22
23
24 (33) Karabatsos, G. J.; Taller, R. A. Structural studies by nuclear magnetic resonance. V.
25
26 phenylhydrazones. *J. Am. Chem. Soc.* **1963**, *85*, 3624-3629.

27
28
29 (34) Palla, G.; Predieri, G.; Domiano, P.; Vignali, C.; Turner, W. Conformational behaviour
30
31 and *E/Z* isomerization of *N*-acyl and *N*-aroylhydrazones. *Tetrahedron* **1986**, *42*, 3649-3654.

32
33
34 (35) Hoffmann, K.; Brosch, G.; Loidl, P.; Jung, M. A non-isotopic assay for histone
35
36 deacetylase activity. *Nucleic Acids Res.* **1999**, *27*, 2057-2058.

37
38
39 (36) Schneider, P.; Hosseiny, S. S.; Szczotka, M.; Jordan, V.; Schlitter, K. Rapid solubility
40
41 determination of the triterpenes oleanolic acid and ursolic acid by UV-spectroscopy in different
42
43 solvents. *Phytochem. Lett.* **2009**, *2*, 85-87.

44
45
46 (37) do Amaral, D. N.; Cavalcanti, B. C.; Bezerra, D. P.; Ferreira, P. M.; Castro Rde, P.;
47
48 Sabino, J. R.; Machado, C. M.; Chammas, R.; Pessoa, C.; Sant'Anna, C. M.; Barreiro, E. J.;
49
50 Lima, L. M. Docking, synthesis and antiproliferative activity of *N*-acylhydrazone derivatives
51
52 designed as combretastatin A4 analogues. *PLoS One* **2014**, *9*, e85380.

1
2
3 (38) Haggarty, S. J.; Tsai, L.-H. Probing the role of HDACs and mechanisms of chromatin-
4 mediated neuroplasticity. *Neurobiol. Learn. Mem.* **2011**, *96*, 41-52.
5
6

7
8 (39) Strahl, B. D.; Allis, C. D. The language of covalent histone modifications. *Nature* **2000**,
9 *403*, 41-45.
10
11

12 (40) Butler, K. V.; Kalin, J.; Brochier, C.; Vistoli, G.; Langley, B.; Kozikowski, A. P.
13 Rational design and simple chemistry yield a superior, neuroprotective HDAC6 inhibitor,
14 tubastatin A. *J. Am. Chem. Soc.* **2010**, *132*, 10842-10846.
15
16
17

18 (41) Wagner, F. F.; Olson, D. E.; Gale, J. P.; Kaya, T.; Weiwer, M.; Aidoud, N.; Thomas,
19 M.; Davoine, E. L.; Lemercier, B. C.; Zhang, Y. L.; Holson, E. B. Potent and selective inhibition
20 of histone deacetylase 6 (HDAC6) does not require a surface-binding motif. *J. Med. Chem.* **2013**,
21 *56*, 1772-1776.
22
23
24
25
26
27

28 (42) Somoza, J. R.; Skene, R. J.; Katz, B. A.; Mol, C.; Ho, J. D.; Jennings, A. J.; Luong, C.;
29 Arvai, A.; Buggy, J. J.; Chi, E.; Tang, J.; Sang, B. C.; Verner, E.; Wynands, R.; Leahy, E. M.;
30 Dougan, D. R.; Snell, G.; Navre, M.; Knuth, M. W.; Swanson, R. V.; McRee, D. E.; Tari, L. W.
31 Structural snapshots of human HDAC8 provide insights into the class I histone deacetylases.
32 *Structure* **2004**, *12*, 1325-1334.
33
34
35
36
37
38

39 (43) Li, L.; Yang, X. J. Tubulin acetylation: responsible enzymes, biological functions and
40 human diseases. *Cell. Mol. Life Sci.* **2015**, *72*, 4237-4255.
41
42
43
44

45 (44) Vannini, A.; Volpari, C.; Filocamo, G.; Casavola, E. C.; Brunetti, M.; Renzoni, D.;
46 Chakravarty, P.; Paolini, C.; De Francesco, R.; Gallinari, P.; Steinkuhler, C.; Di Marco, S.
47 Crystal structure of a eukaryotic zinc-dependent histone deacetylase, human HDAC8, complexed
48 with a hydroxamic acid inhibitor. *Proc. Natl. Acad. Sci. U. S. A.* **2004**, *101*, 15064-15069.
49
50
51
52
53
54
55
56
57
58
59
60

1
2
3 (45) Biasini, M.; Bienert, S.; Waterhouse, A.; Arnold, K.; Studer, G.; Schmidt, T.; Kiefer, F.;
4
5 Cassarino, T. G.; Bertoni, M.; Bordoli, L.; Schwede, T. SWISS-MODEL: modelling protein
6
7 tertiary and quaternary structure using evolutionary information. *Nucleic Acids Res.* **2014**, *42*,
8
9 W252-W258.
10

11
12 (46) Benkert, P.; Biasini, M.; Schwede, T. Toward the estimation of the absolute quality of
13
14 individual protein structure models. *Bioinformatics* **2011**, *27*, 343-350.
15

16
17 (47) Arnold, K.; Bordoli, L.; Kopp, J.; Schwede, T. The SWISS-MODEL workspace: a web-
18
19 based environment for protein structure homology modelling. *Bioinformatics* **2006**, *22*, 195-201.
20

21
22 (48) Schuetz, A.; Min, J.; Allali-Hassani, A.; Schapira, M.; Shuen, M.; Loppnau, P.;
23
24 Mazitschek, R.; Kwiatkowski, N. P.; Lewis, T. A.; Maglathin, R. L.; McLean, T. H.; Bochkarev,
25
26 A.; Plotnikov, A. N.; Vedadi, M.; Arrowsmith, C. H. Human HDAC7 harbors a class IIa histone
27
28 deacetylase-specific zinc binding motif and cryptic deacetylase activity. *J. Biol. Chem.* **2008**,
29
30 *283*, 11355-11363.
31

32
33 (49) El-Serag, H. B. Hepatocellular carcinoma. *N. Engl. J. Med.* **2011**, *365*, 1118-1127.
34

35
36 (50) Kanno, K.; Kanno, S.; Nitta, H.; Uesugi, N.; Sugai, T.; Masuda, T.; Wakabayashi, G.;
37
38 Maesawa, C. Overexpression of histone deacetylase 6 contributes to accelerated migration and
39
40 invasion activity of hepatocellular carcinoma cells. *Oncol. Rep.* **2012**, *28*, 867-873.
41

42
43 (51) Ding, G.; Liu, H. D.; Huang, Q.; Liang, H. X.; Ding, Z. H.; Liao, Z. J.; Huang, G.
44
45 HDAC6 promotes hepatocellular carcinoma progression by inhibiting P53 transcriptional
46
47 activity. *FEBS Lett.* **2013**, *587*, 880-886.
48

49
50 (52) Bergman, J. A.; Woan, K.; Perez-Villarroel, P.; Villagra, A.; Sotomayor, E. M.;
51
52 Kozikowski, A. P. Selective histone deacetylase 6 inhibitors bearing substituted urea linkers
53
54 inhibit melanoma cell growth. *J. Med. Chem.* **2012**, *55*, 9891-9899.
55
56
57
58
59
60

1
2
3 (53) Lakshmaiah, K. C.; Jacob, L. A.; Aparna, S.; Lokanatha, D.; Saldanha, S. C. Epigenetic
4 therapy of cancer with histone deacetylase inhibitors. *J. Cancer Res. Ther.* **2014**, *10*, 469-478.
5

6
7
8 (54) Hubbert, C.; Guardiola, A.; Shao, R.; Kawaguchi, Y.; Ito, A.; Nixon, A.; Yoshida, M.;
9 Wang, X.-F.; Yao, T.-P. HDAC6 is a microtubule-associated deacetylase. *Nature* **2002**, *417*,
10 455-458.
11
12

13
14
15 (55) Zhang, Y.; Li, N.; Caron, C.; Matthias, G.; Hess, D.; Khochbin, S.; Matthias, P. HDAC-
16 6 interacts with and deacetylates tubulin and microtubules in vivo. *EMBO J.* **2003**, *22*, 1168-
17 1179.
18
19

20
21
22 (56) Blagosklonny, M. V.; Robey, R.; Sackett, D. L.; Du, L.; Traganos, F.; Darzynkiewicz,
23 Z.; Fojo, T.; Bates, S. E. Histone deacetylase inhibitors all induce p21 but differentially cause
24 tubulin acetylation, mitotic arrest, and cytotoxicity. *Mol. Cancer Ther.* **2002**, *1*, 937-941.
25
26

27
28
29 (57) Richon, V. M.; Sandhoff, T. W.; Rifkind, R. A.; Marks, P. A. Histone deacetylase
30 inhibitor selectively induces p21WAF1 expression and gene-associated histone acetylation.
31
32
33
34 *Proc. Natl. Acad. Sci. U. S. A.* **2000**, *97*, 10014-10019.
35

36
37 (58) Zhao, Y.; Tan, J.; Zhuang, L.; Jiang, X.; Liu, E. T.; Yu, Q. Inhibitors of histone
38 deacetylases target the Rb-E2F1 pathway for apoptosis induction through activation of
39 proapoptotic protein Bim. *Proc. Natl. Acad. Sci. U. S. A.* **2005**, *102*, 16090-16095.
40
41
42

43
44 (59) Zhang, X. D.; Gillespie, S. K.; Borrow, J. M.; Hersey, P. The histone deacetylase
45 inhibitor suberic bishydroxamate regulates the expression of multiple apoptotic mediators and
46 induces mitochondria-dependent apoptosis of melanoma cells. *Mol. Cancer Ther.* **2004**, *3*, 425-
47 435.
48
49
50

51
52
53 (60) Fandy, T. E.; Shankar, S.; Ross, D. D.; Sausville, E.; Srivastava, R. K. Interactive effects
54 of HDAC inhibitors and TRAIL on apoptosis are associated with changes in mitochondrial
55
56
57
58
59
60

1
2
3 functions and expressions of cell cycle regulatory genes in multiple myeloma. *Neoplasia* **2005**, *7*,
4
5 646-657.
6

7
8 (61) Clayden, J.; Greeves, N.; Warren, S. G. *Organic chemistry*. 2nd ed.; Oxford University
9
10 Press: Oxford, NY, 2012.
11

12 (62) Martinez, C. H.; Dardonville, C. Rapid determination of ionization constants (pKa) by
13
14 UV spectroscopy using 96-well microtiter plates. *ACS Med. Chem. Lett.* **2013**, *4*, 142-145.
15

16
17 (63) Monzyk, B.; Crumbliss, A. L. Acid dissociation constants (Ka) and their temperature
18
19 dependencies (.DELTA.Ha, .DELTA.Sa) for a series of carbon- and nitrogen-substituted
20
21 hydroxamic acids in aqueous solution. *J. Org. Chem.* **1980**, *45*, 4670-4675.
22
23

24 (64) Cory, A. H.; Owen, T. C.; Barltrop, J. A.; Cory, J. G. Use of an aqueous soluble
25
26 tetrazolium/formazan assay for cell growth assays in culture. *Cancer Commun.* **1991**, *3*, 207-212.
27
28

29 (65) Zanin, J. L.; Massoni, M.; Santos, M. H.; Freitas, G. C.; Niero, E. L.; Schefer, R. R.;
30
31 Lago, J. H.; Ionta, M.; Soares, M. G. Caesalpinioflavone, a new cytotoxic biflavonoid Isolated
32
33 from *Caesalpinia pluviosa* var. *peltophoroides*. *J. Braz. Chem. Soc.* **2015**, *26*, 804-809.
34
35

36 (66) Mooij, W. T.; Verdonk, M. L. General and targeted statistical potentials for protein-
37
38 ligand interactions. *Proteins* **2005**, *61*, 272-287.
39

40 (67) Korb, O.; Stutzle, T.; Exner, T. E. Empirical scoring functions for advanced protein-
41
42 ligand docking with PLANTS. *J. Chem. Inf. Model.* **2009**, *49*, 84-96.
43
44

45 (68) Eldridge, M.; Murray, C.; Auton, T.; Paolini, G.; Mee, R. Empirical scoring functions: I.
46
47 the development of a fast empirical scoring function to estimate the binding affinity of ligands in
48
49 receptor complexes. *J. Comput. Aid. Mol. Des.* **1997**, *11*, 425-445.
50
51
52
53
54
55
56
57
58
59
60

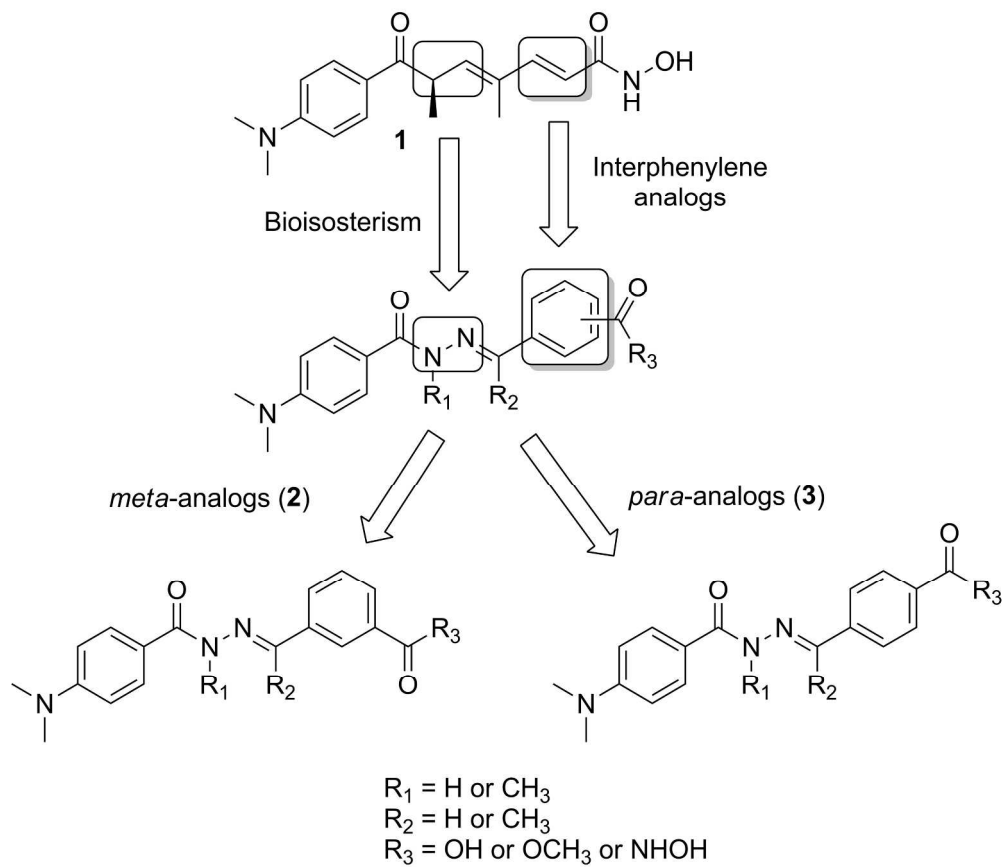
1
2
3 (69) Baxter, C. A.; Murray, C. W.; Clark, D. E.; Westhead, D. R.; Eldridge, M. D. Flexible
4 docking using tabu search and an empirical estimate of binding affinity. *Proteins* **1998**, *33*, 367-
5
6 382.
7
8

9
10 (70) Jones, G.; Willett, P.; Glen, R. C. Molecular recognition of receptor sites using a genetic
11 algorithm with a description of desolvation. *J. Mol. Biol.* **1995**, *245*, 43-53.
12
13

14 (71) Jones, G.; Willett, P.; Glen, R. C.; Leach, A. R.; Taylor, R. Development and validation
15 of a genetic algorithm for flexible docking. *J. Mol. Biol.* **1997**, *267*, 727-748.
16
17
18

19 (72) Lovell, S. C.; Davis, I. W.; Arendall, W. B., 3rd; de Bakker, P. I.; Word, J. M.; Prisant,
20 M. G.; Richardson, J. S.; Richardson, D. C. Structure validation by Calpha geometry: phi,psi and
21 Cbeta deviation. *Proteins* **2003**, *50*, 437-450.
22
23
24
25
26
27
28
29
30
31
32
33
34
35
36
37
38
39
40
41
42
43
44
45
46
47
48
49
50
51
52
53
54
55
56
57
58
59
60

1
2
3
4
5
6
7
8
9
10
11
12
13
14
15
16
17
18
19
20
21
22
23
24
25
26
27
28
29
30
31
32
33
34
35
36
37
38
39
40
41
42
43
44
45
46
47
48
49
50
51
52
53
54
55
56
57
58
59
60



36 Figure 2. Design concept used to generate a novel class of NAH derivatives for the inhibition of HDACs.
37 115x99mm (600 x 600 DPI)

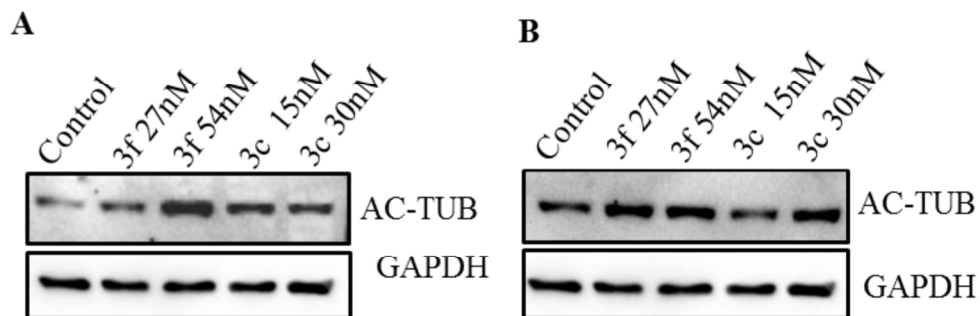
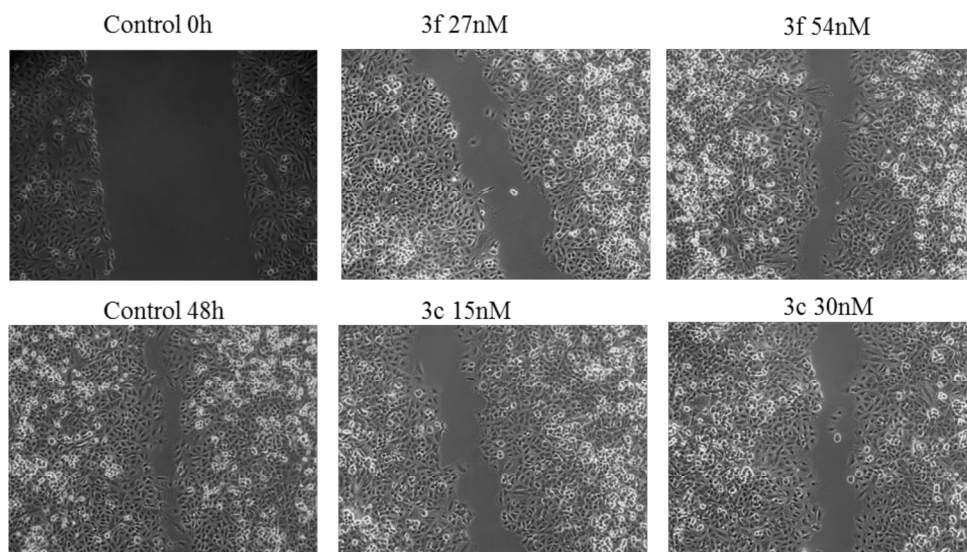


Figure 3. HDACi enhances tubulin acetylation. Calu-1 (A) and A549 (B) cells were treated with compounds 3c and 3f for 24 h, and the levels of acetylated tubulin were accessed by western blotting. GAPDH was used as a loading control. One representative of three independent experiments is shown. Cells treated with vehicle (DMSO) were used as controls.

129x44mm (300 x 300 DPI)



26
27
28
29
30
31
32
33
34
35
36
37
38
39
40
41
42
43
44
45
46
47
48
49
50
51
52
53
54
55
56
57
58
59
60

Figure 4. HDAC6 inhibition abrogates cell migration. Calu-1 cells were treated with compounds 3c and 3f for 48 h, and their migration was determined using the scratch test. One representative of three independent experiments is shown. Cells treated with vehicle (DMSO) were used as controls.
168x95mm (300 x 300 DPI)

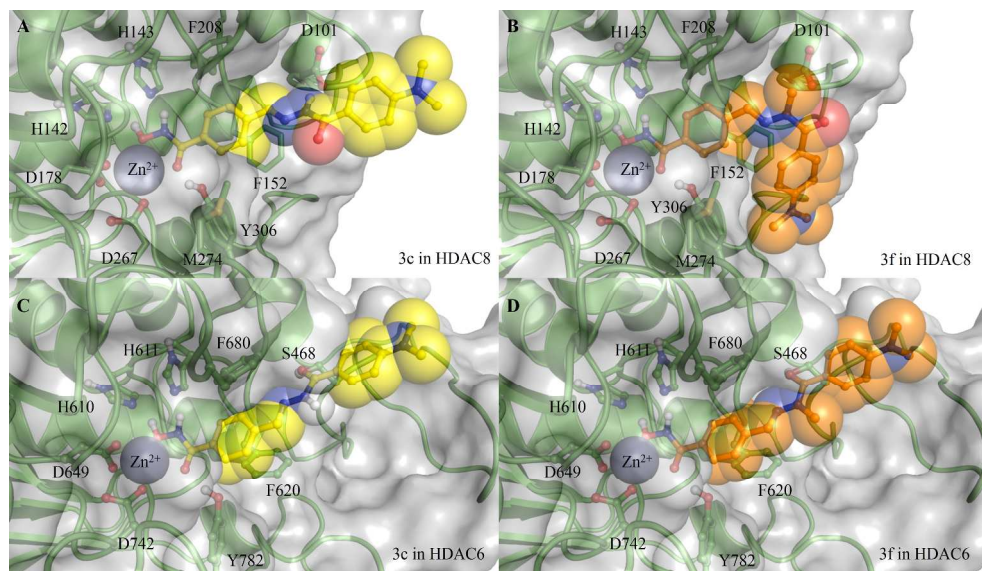


Figure 5. Compounds 3c and 3f docked into HDAC8 (A, B) and HDAC6 (C, D). Docking studies were performed by using the program GOLD 5.1.
338x190mm (300 x 300 DPI)

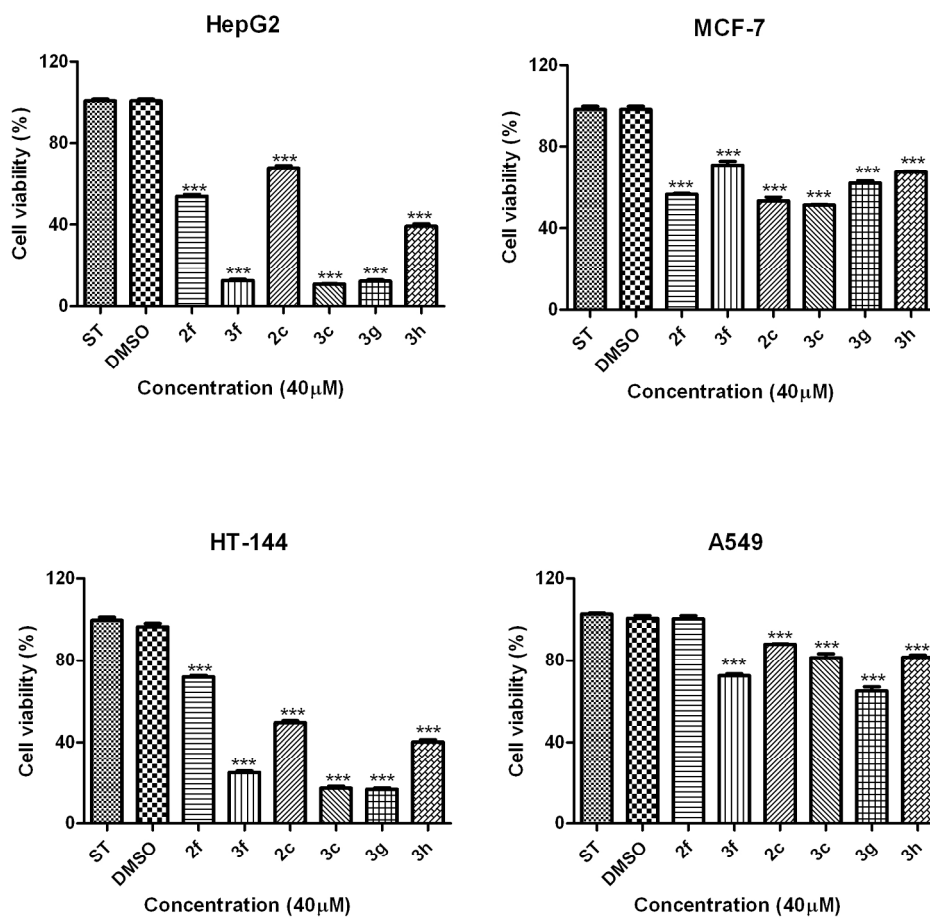


Figure 6. Cell viability determined using the MTS assay after 48 h of treatment with different compounds at 40 μM. The significance of the differences compared with the control groups were determined by ANOVA followed by Tukey's post-test. *** p < 0.001.
190x186mm (300 x 300 DPI)

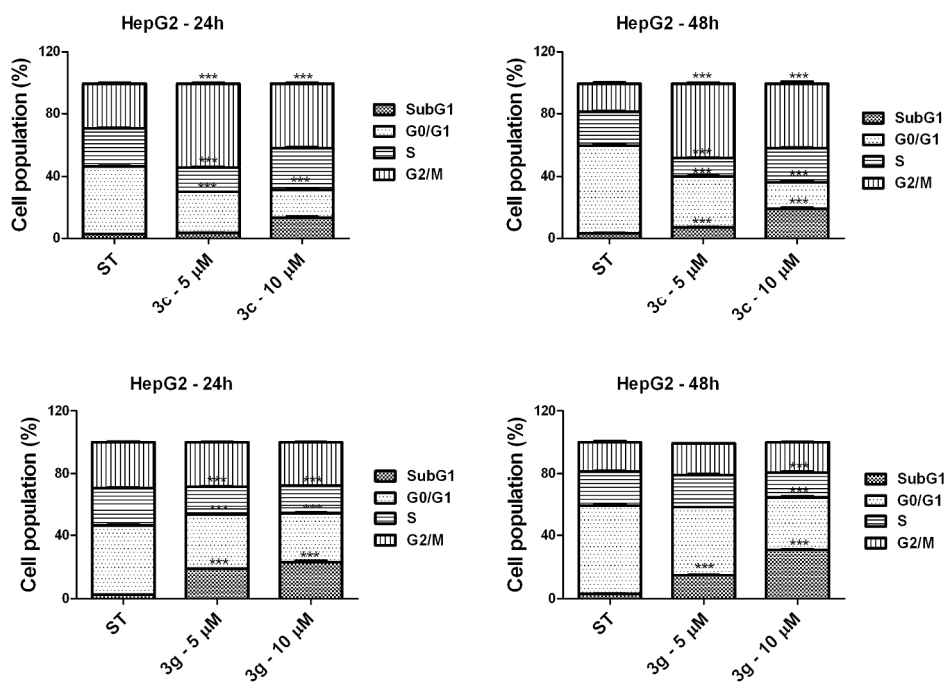


Figure 7. Cell cycle analysis of HepG2 cells treated with compounds 3c and 3g at concentrations of 5 and 10 μM for 24 and 48 h. The significance of the differences compared with the control results were determined by ANOVA followed by Tukey's post-test. *** p < 0.001.
241x176mm (300 x 300 DPI)

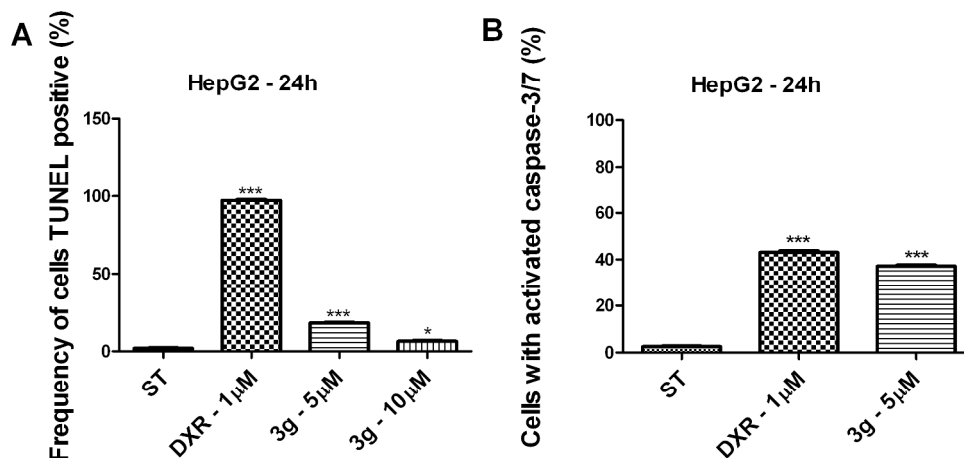


Figure 8. Frequency of apoptotic cells determined through a TUNEL assay (A), and the caspase 3/7 activation profile (B) in HepG2 cell cultures treated for 24 h with compound 3g. Doxorubicin (DXR) was used as a positive control. The significance of the differences compared with the control results were determined by ANOVA followed by Tukey's post-test. * $p < 0.05$ and *** $p < 0.001$.

273x140mm (300 x 300 DPI)

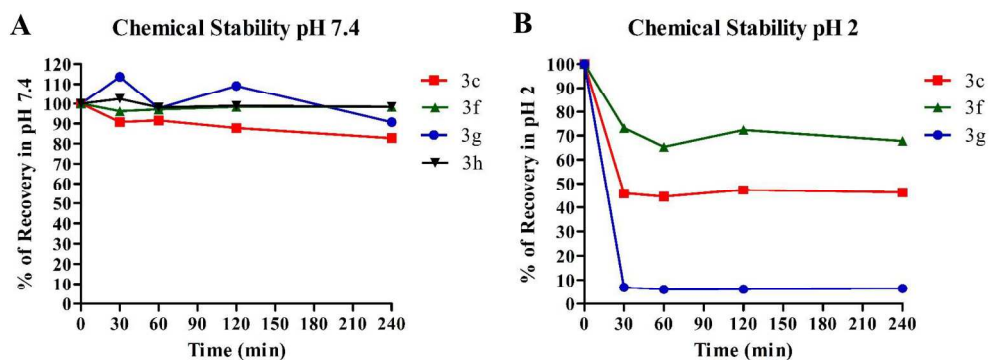
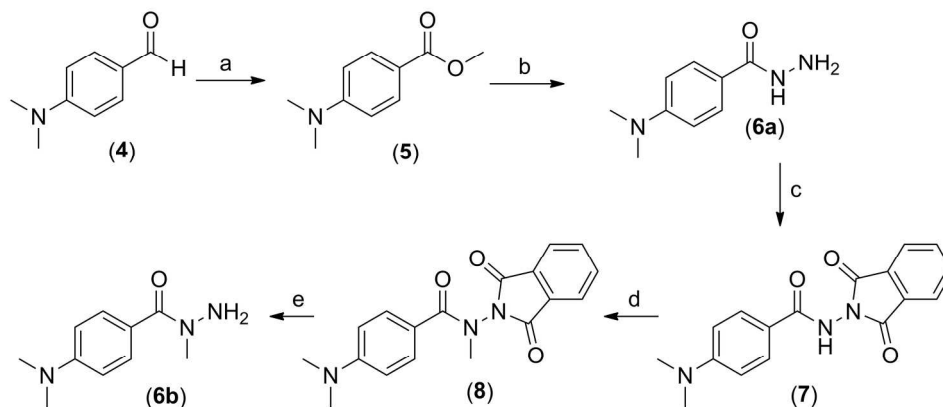


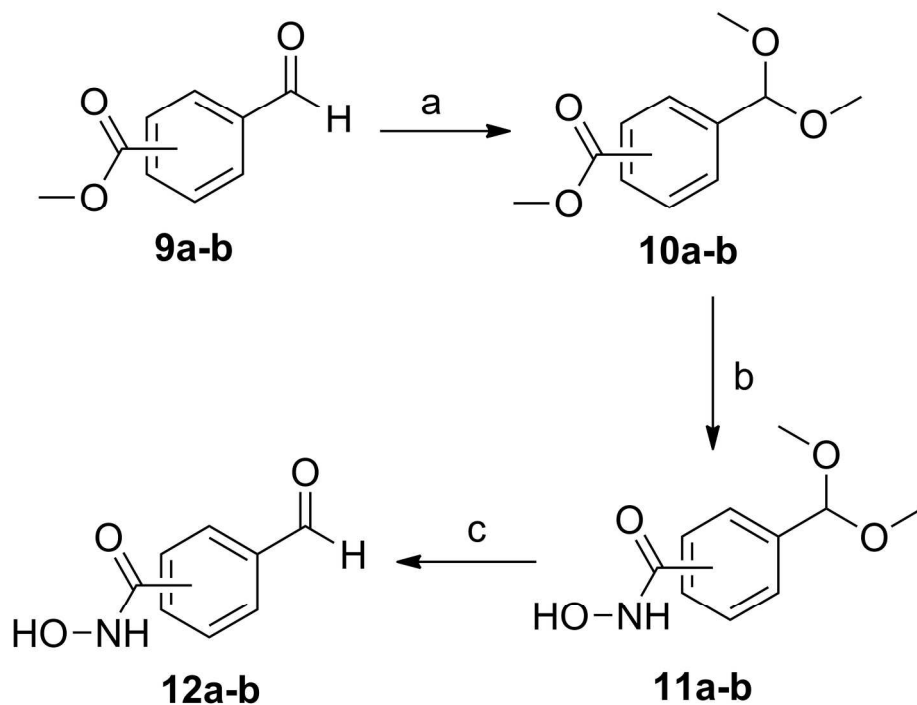
Figure 9. Chemical stability of compounds 3c, 3f, 3g and 3h. A) Chemical stability of compounds 3c, 3f, 3g and 3h at pH 7.4. B) Chemical stability of compounds 3c, 3f, 3g and 3h at pH 2. The experiments were conducted in triplicate, and the values shown represent the average from the experiments.

210x82mm (300 x 300 DPI)

Scheme 1^a

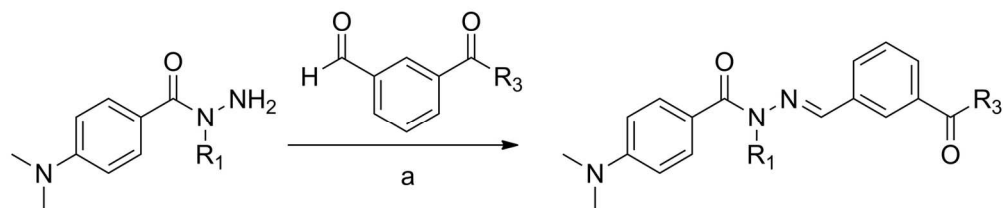
^aReagents and conditions: (a) I₂, KOH, MeOH, 0 °C, 10 h, 57%; (b) NH₂NH₂·H₂O, MeOH, 70 °C, 18 h, 95%; (c) phthalic anhydride, 180 °C, 2 h, 76%; (d) CH₃I, K₂CO₃, acetone, 50 °C, 18 h, 92%; (e) NH₂NH₂·H₂O, MeOH, 70 °C, 2 h, 79%

Scheme 1
94x56mm (600 x 600 DPI)

Scheme 2^a

^aReagents and conditions: (a) 2,2-dimethoxypropane, TsOH_{cat.}, MeOH, r.t., 2 h, 82-85%; (b) NH₂OH·HCl, KOH, MeOH, r.t., 4 h, 90-94%; (c) H₂SO₄ 15% (w/v), acetone, r.t., 2 h, 87-91%.

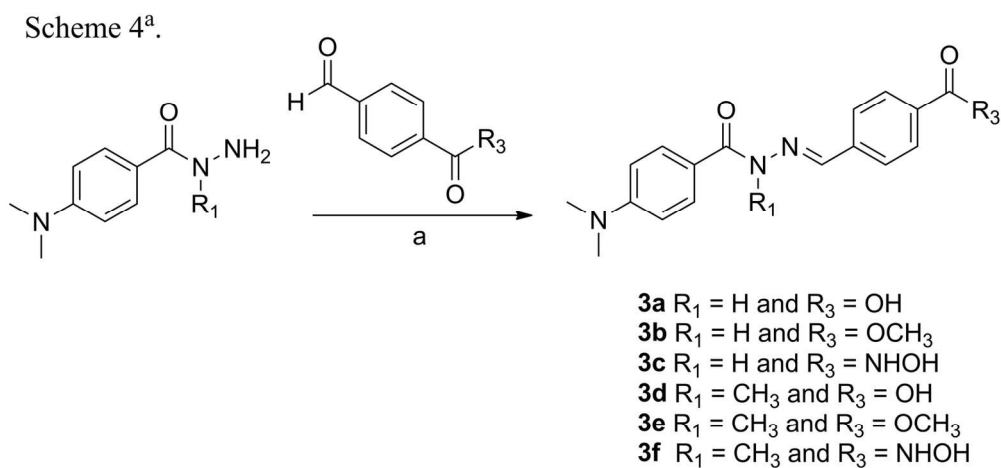
Scheme 2
100x109mm (600 x 600 DPI)

1
2
3
4
5
6
7
8
9
10
11
12
13
14
15
16
17
18
19
20
21
22
23
24
25
26
27
28
29
30
31
32
33
34
35
36
37
38
39
40
41
42
43
44
45
46
47
48
49
50
51
52
53
54
55
56
57
58
59
60Scheme 3^a.

- 2a** R₁ = H and R₃ = OH
2b R₁ = H and R₃ = OCH₃
2c R₁ = H and R₃ = NHOH
2d R₁ = CH₃ and R₃ = OH
2e R₁ = CH₃ and R₃ = OCH₃
2f R₁ = CH₃ and R₃ = NHOH

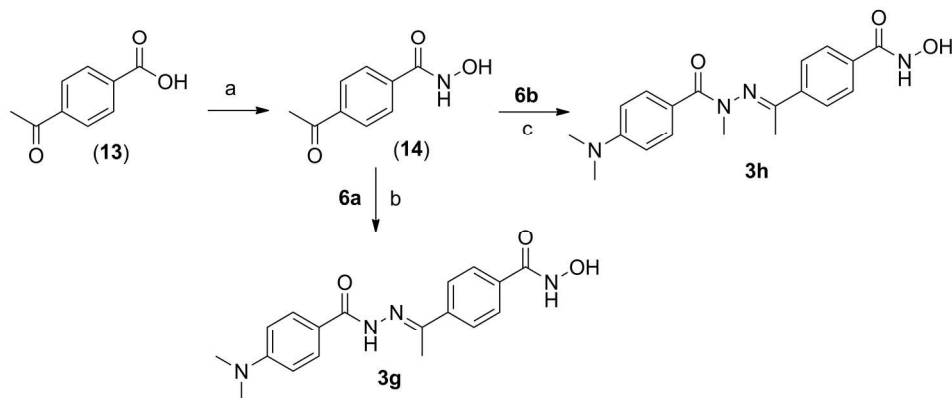
^aReagents and conditions: (a) HCl_{cat.}, EtOH, r.t., 2 h, 82-98%;

Scheme 3
74x40mm (600 x 600 DPI)



^aReagents and conditions: (a) HCl_{cat.}, EtOH, r.t., 2 h, 62-89%;

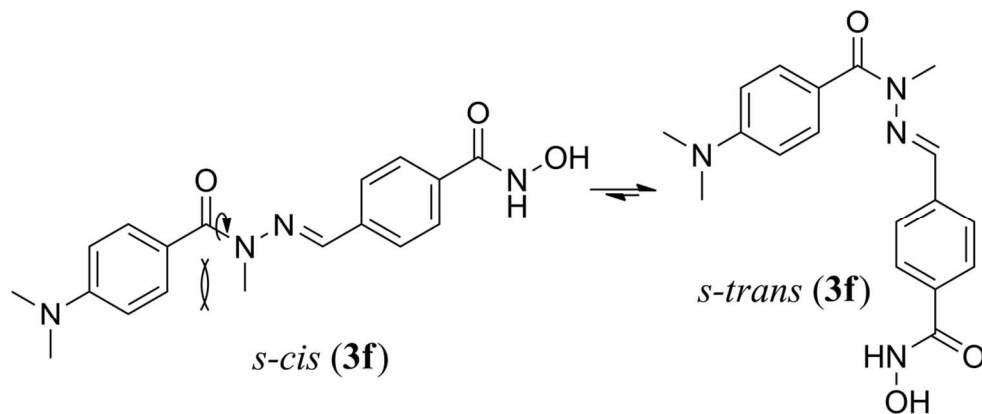
Scheme 4
73x39mm (600 x 600 DPI)

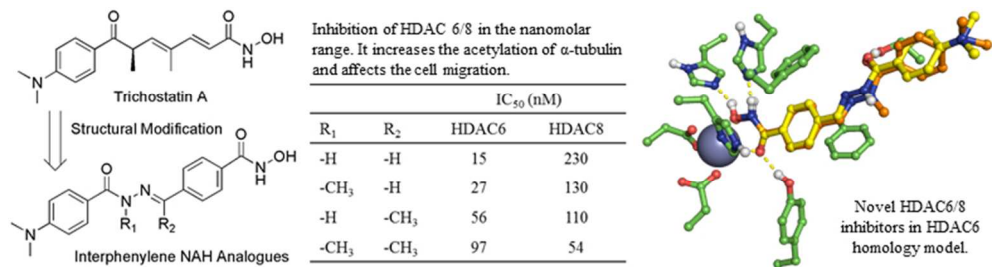
Scheme 5^a.

^aReagents and conditions: (a) Oxalyl chloride, DMF_{cat}, DCM, r.t., 2 h, then 50 wt % NH₂OH, TEA, THF, 0 °C, 30 min, 54%. (b) AcOH_{cat}, EtOH, 80 °C, MW, 30 min, 45%; (c) AcOH_{cat}, EtOH, 125 °C, MW, 4 h, 38%.

Scheme 5
99x58mm (600 x 600 DPI)

Scheme 6.

Scheme 6
56x28mm (600 x 600 DPI)



16
17
18
19
20
21
22
23
24
25
26
27
28
29
30
31
32
33
34
35
36
37
38
39
40
41
42
43
44
45
46
47
48
49
50
51
52
53
54
55
56
57
58
59
60

TOC graphic
210x55mm (96 x 96 DPI)